EXPLORATORY ELECTROMAGNETIC THRUSTER RESEARCH

by
A. C. Ducati, R. G. Jahn, E. Muehlberger
and R. P. Treat

prepared for

NATIONAL AERONAUTICS AND SPACE ADMINISTRATION
CONTRACT NAS w-1513

GIANNINI SCIENTIFIC CORPORATION
Santa Ana, California

N68-21901
(ACCESSION NUMBER)   (THRU)
75   /
(PAGES)   (CODE)
NASA CR # 62047   28
(NASA CR OR TMX OR AD NUMBER)   (CATEGORY)

FACILITY FORM 602

ANNUAL REPORT
TR 117-1513

EXPLORATORY ELECTROMAGNETIC THRUSTER RESEARCH

by
A. C. Ducati, R. G. Jahn, E. Muehlberger
and R. P. Treat

prepared for

NATIONAL AERONAUTICS AND SPACE ADMINISTRATION
Washington, D. C.

CONTRACT NAS w-1513

February 1968

GIANNINI SCIENTIFIC CORPORATION
Santa Ana, California

FOREWORD

This is the annual report on work carried out during the period 12 September 1966 to 31 January 1968 by Giannini Scientific Corporation on "Exploratory Electromagnetic Thruster Research," Contract NAS w-1513, originating in the Electrothermal and Electromagnetic Section, Washington, D. C. under the direction of Jerome P. Mullin.

Adriano C. Ducati was the Principal Investigator in charge of the direction of the work and preparation of the report. The theoretical analysis presented is by R. G. Jahn and R. P. Treat. Erich Muehlberger was active in all phases of the experimental effort. Ernest Dageford contributed to the design and installation of the new insulating vacuum facility.

ABSTRACT

A cylindrical fiberglass tank 25 feet long and 10 feet in diameter has been constructed and tested. Pressures between 10^{-5} and 10^{-4} torr are obtained with a 0.1 to 1 mg/sec H_2 mass flow. The structural and vacuum properties of the tank are entirely satisfactory. The thrust stand is aerodynamically and electromagnetically isolated from the tank environment. Provision has been made for the interchange of thruster and thruster components while maintaining a high vacuum. Initial tests in the high vacuum insulated tank are discussed. An analysis of the arc has been conducted by means of an analytical model which assumes only electromagnetic forces. The analysis yields the plasma motion and current density variation following the motion of a plasma element through the discharge. A re-examination of the use of an external magnetic field to improve performance is given. Various aspects of the external field interactions are presented.

TABLE OF CONTENTS

LIST OF ILLUSTRATIONS

SUMMARY

A new fiberglass cylindrical vacuum tank 25 feet long and 10 feet in diameter is described. The vacuum is obtained with mechanical forepumps and a 140,000 liter/sec diffusion pump. Pressures between 10^{-5} and 10^{-4} torr are obtained with hydrogen mass flows from 0.1 to 2 mg/sec injected into the tank. The leak and outgasing are equivalent to a flow rate less than a 0.01 mg/sec hydrogen flow, showing the fiberglass construction and vacuum characteristics are entirely satisfactory in the range of mass flow intended for our MPD thruster application. The design and construction of a new thrust stand is discussed. The design provides for the aerodynamic and electromagnetic isolation of the thrust stand from the tank environment. A provision has been made for the interchange of thrusters and thruster components while maintaining a high vacuum, thereby avoiding lengthy pump-down periods. A thruster has been operated in the new tank with a 1 mg/sec mass flow of about 8 kw arc power over a range of magnetic field strengths. A very distinct cathodic discharge extends axially well away from the thruster, then turns toward the wall where it appears to form the first turn of a spiraling discharge toward the end of the tank. Reversing the direction of the magnetic coil current reverses the sense of the spiralling. The separation of the cathodic discharge and the usual bell-shaped plume becomes less distinct as the magnetic field is increased and at very strong fields the arc discharge acquires a diffuse appearance. In these first tests the dependence of the arc voltage on magnetic field strength is found to be somewhat different than has previously been observed, but further tests are necessary to confirm this result.

An analysis of the MPD arc has been conducted for the case of a strong applied magnetic field by means of an analytical model which assumes steady flow, charge neutrality, incompressibility, uniform electric and magnetic fields, considers only electromagnetic forces in both the momentum and the current equation and neglects the self field of the arc currents. The analysis, carried out in Lagrangian coordinates, yields the plasma motion and current density as a function of the initial coordinates and time following the motion of a plasma element. If the solution, which has been obtained for plane parallel electordes with crossed electric and magnetic fields, is applied to a coaxial geometry, a plasma element is found to follow a spiraling motion with superimposed damped radial and azimuthal spatial oscillations. The damped oscillatory radial motion tends to zero velocity with a net displacement toward the axis of the configuration and the azimuthal motion tends to the drift velocity.

We have also conducted a basic re-examination of the use of external magnetic fields to improve arc jet performance. The thoughts presented are advanced in the spirit of encouraging more detailed study of certain aspects of the external field interactions before categorically accepting the logistical complications and propulsion system disadvantages which accompany the strong field. Points have been raised which pertain to 1) the need for a more precise classification of arcs with respect to electrode geometry and arc mode before

attempting correlation of performance data, 2) the efficiency of the arc in the spoked mode of operation, 3) the effectiveness of an external field in providing streamwise acceleration, and 4) characteristics of the arc which suggest a tendency toward equipartition of ionization potential energy and kinetic energy in the arc.

1.0 INTRODUCTION

During this period the experimental work consisted mostly of the designing and testing of a facility devised to create an environment for arc thrusters which simulates space as closely as is permitted by technical and economic limitations. The choice of an insulated tank for the test environment with the largest dimensions allowed by the available funding (10 by 25 feet) has been made in an attempt to avoid electromagnetic interactions with the tank and aerodynamic interference caused by the proximity of the tank walls. With a pumping capacity of 1.4×10^5 liters/sec and a high conductance connection to the tank vacuum pressures in the range of 10^{-4} to 10^{-5} torr are obtained when mass flows of 0.1 to 1.0 mg/sec of hydrogen are injected. Admitting that for a simulation of even rather low altitude space conditions lower pressures and larger tank dimensions would be required, the new facility represents a compromise where we hope to achieve reliable test results. Originally a glass vacuum tank was planned but because of practical difficulties with glass for large diameter tanks, a construction of fiberglass has been adopted. The design of the fiberglass tank was based on tests with a scaled-down model which showed satisfactory characteristics. In Section 2.1 the construction of the new tank is described, the vacuum properties discussed and the vacuum attainable as a function of mass flow is given.

Together with the development of the tank and its vacuum system we have proceeded with the design and construction of a thrust stand which should not be susceptible to spurious aerodynamic and electromagnetic forces. This new thrust stand has a rather unconventional design as it is electrically and aerodynamically isolated from the vacuum tank environment. Together with this new type of thrust stand a provision for the interchange of thrusters and components without pumping down the main tank has been provided. This will permit a tenfold increase in the number of tests that can be conducted during a determined length of time. The design and construction of the new thrust stand is discussed and drawings of this insulated thrust stand and accessory components are shown in Section 2.2. A thruster has been operated in the new tank at a 1 mg/sec mass flow rate and tank pressure of 4.0×10^{-5} torr. In these preliminary tests the arc has operated stably and continuously at about 8 kilowatts arc power over a range of magnetic field strengths. The appearance of the arc and the results of these preliminary tests are discussed in Section 2.3. A complete series of tests will be made and the performance compared with thruster data obtained in smaller metal tanks.

The development of the coaxial arc jet for plasma acceleration has been primarily an empirical process, and the accumulated bulk of terminal performance data far outweighs any detailed understanding of the physical mechanisms prevailing in such devices. While perhaps justifiable on the basis of the complexity of the phenomena, the multivaried significant parameters, and the urgency of application in several technologies, this empiricism, unless

3

regularly supplemented by incisive research, can lead to entrenchment of inferior techniques on no firmer basis than simple familiarity or local convenience. One technique requiring such basic re-examination is the use of external magnetic fields to improve arc jet performance for propulsion. In Section 3.1 a discussion of central problems associated with the use of the external field is given. The thoughts presented here by no means resolve any of the ambiguities of the MPD arc, nor provide a definitive answer to the question of the usefulness of a strong field. Rather they are advanced in the spirit of encouraging more detailed study of certain aspects of the external magnetic field interactions before categorically accepting the logistical complications and propulsion system disadvantages of these techniques.

In Section 3.2 we undertake the theoretical analysis of the spatial distribution of the arc current density. In the MPD arc, an unionized element of gas flows into a region where the discharge forms and then flows through the discharge and is finally ejected in a current-free, strongly ionized, electrically neutral, axially directed jet. During and after the ionization, pressure gradients and Lorentz forces accelerate the element until the electric field viewed from a coordinate frame moving with the gas element vanishes. In this investigation we consider the growth and decay of the current density following an arbitrary gas element through the discharge. In the analysis we acknowledge the ionization and acceleration of the gas and its effect on the current density variation. The case where the applied field is strong compared with the fields induced by the arc currents and the magnetic pressure is comparable to or larger than the plasma kinetic pressure is considered. One of the results of the analysis is an indication of a mechanism for the suppression of the Hall current density and the enhancement of the radial current density in regions of large Hall parameter.

2.0 EXPERIMENTAL PROGRAM

2.1 Construction and Test of an Insulated Vacuum Tank

The principal design characteristics of the insulated vacuum tank constructed during the initial period of this contract have been described in Reference 1. For convenience we repeat here some of the important design features.

The design of the vacuum tank shown in Figure 1 includes 24 sealed windows distributed along the walls of the tank to permit optical observation in any direction and the insertion of diagnostic probes. The inside of the tank has been made opaque black in order to form a uniform contrasting background when picutres are taken; the outside is white. A cooling system with plastic tubes imbedded in the insulation has been designed but has not been included in this construction for reasons of cost. A cooling system is, however, a good and simple way to improve the minimum vacuum attainable and to permit the testing of higher power thrusters. Another solution studied is to place the refrigerant or the refrigerating coils outside the tank walls so as to permit a simpler construction and an easier inspection.

The construction of the insulating tank was initiated from the inside with a gradual building up of the thickness of the walls. For this reason the first layer, which is constantly in intimate contact with the tank vacuum, is the most important surface. A metal form was used for the initiation of the construction and as soon as a substantially rigid layer of plastic material was deposited on the metal surface, the form was taken away and the buildup of the successive layers was made directly on the first. The windows were made when the tank was completely finished. To improve the angle of view from each window the sealing flanges have been connected directly to the tank surface eliminating any intermediate pipe. This feature, which is desirable for taking wide angle pictures, does slightly increase the cost of the finished tank. The basic material used in the tank is a polyester resin combined with ordinary fiberglass. The distribution of the various layers of plastics is as follows: The first layer sprayed over the mandrel is a black gel coat of polyester material containing a small percentage of carbon black. The high reactivity of this material gives a higher density and a reduced outgasing. A layer of fiberglass is sprayed over this first support as soon as the mandrel is removed and when this is terminated a rigid isophthalic polyester resin of high reactivity is superimposed. It has an especially long gel time adapted for the fabrication of very large parts and the high reactivity permits reducing the outgasing under vacuum to the minimum. Immediately over this laminating resin a layer of fiberglass woven roving is applied followed by another glaze coat of polyester. Finally a white gel coat of polyester is sprayed to produce the final surface of the tank. The finished tank has the appearance illustrated in Figures 2 through 4 while Figures 5 through 7 show the complete installation with a 52-inch vacuum diffusion pump connected vertically at the end.

1. Laboratory floor
2. Fiberglass vacuum tank
3. Connecting flange to thrust stand
4. Re-enforcement ribs
5. Viewing windows
6. Drain

7. Tank support
8. Laboratory floor excavation
9. Connecting elbow to diffusion pump
10. Diffusion pump
11. Pump support
12. Vacuum foreline manifold connecting to high capacity and standby forepumps
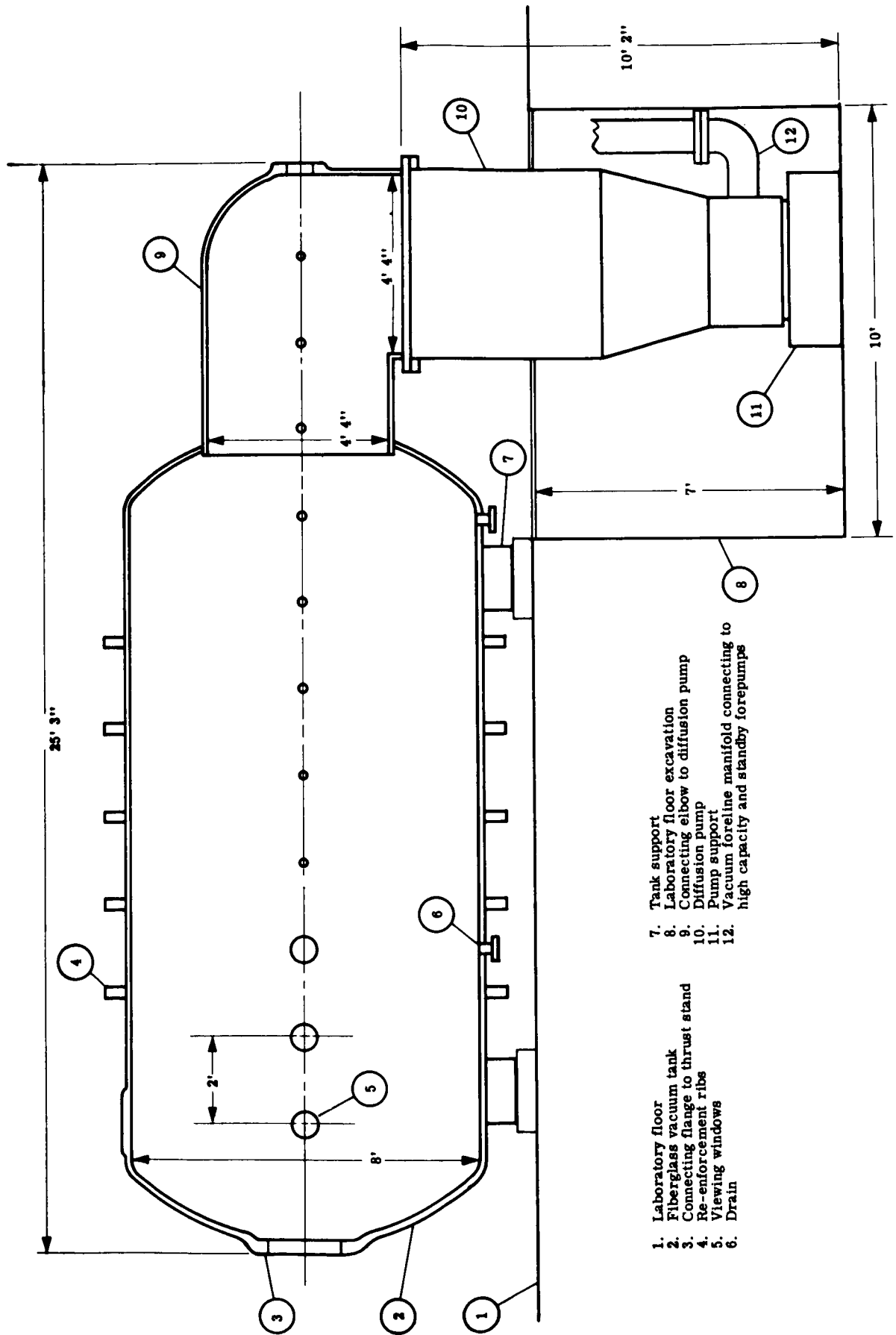
Figure 1. Schematic of High Vacuum Facility Installation

6

Figure 2. Side View of Fiberglass Vacuum Chamber Prior to Installation
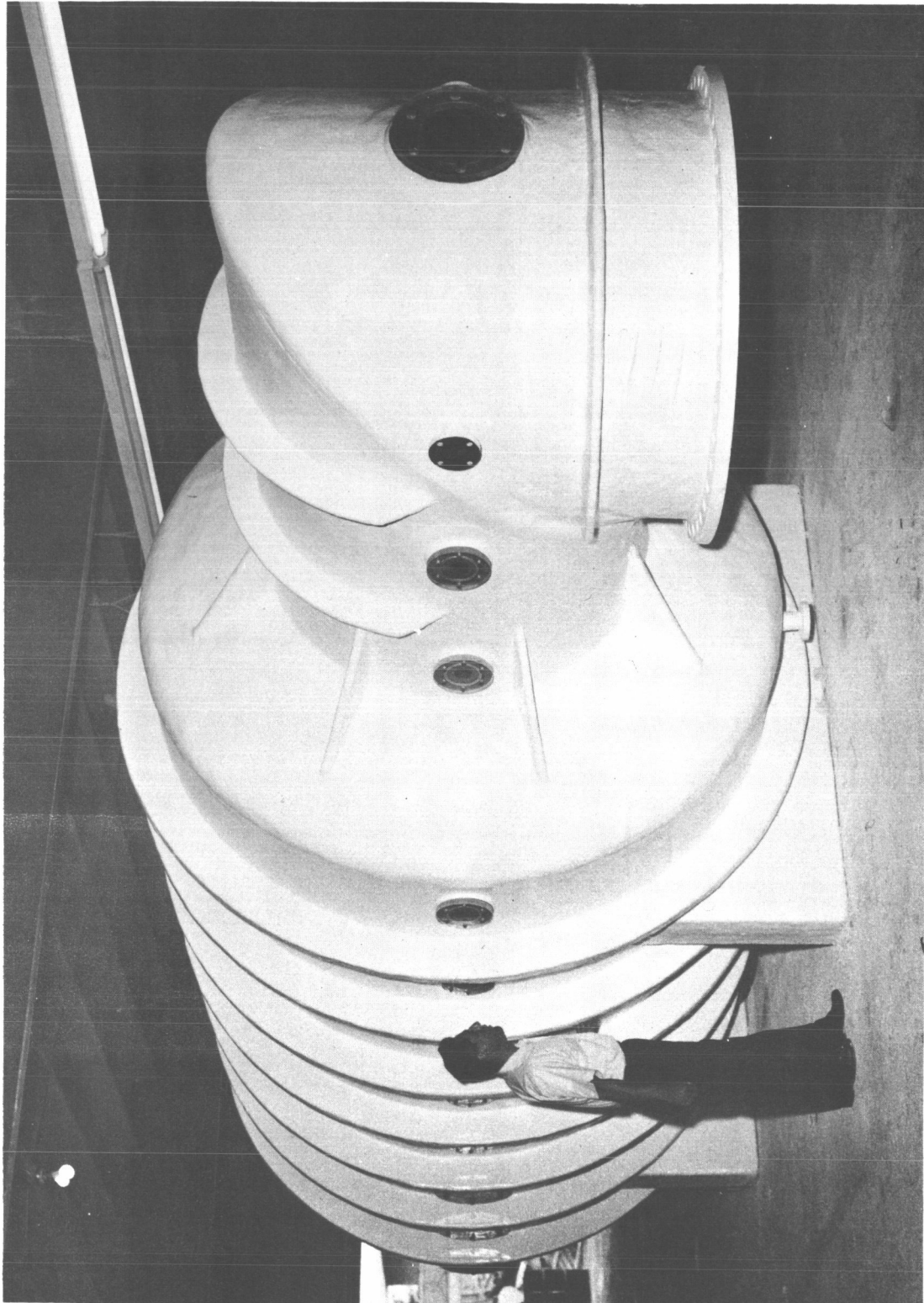
Figure 4. End and Side View of Fiberglass Vacuum Chamber
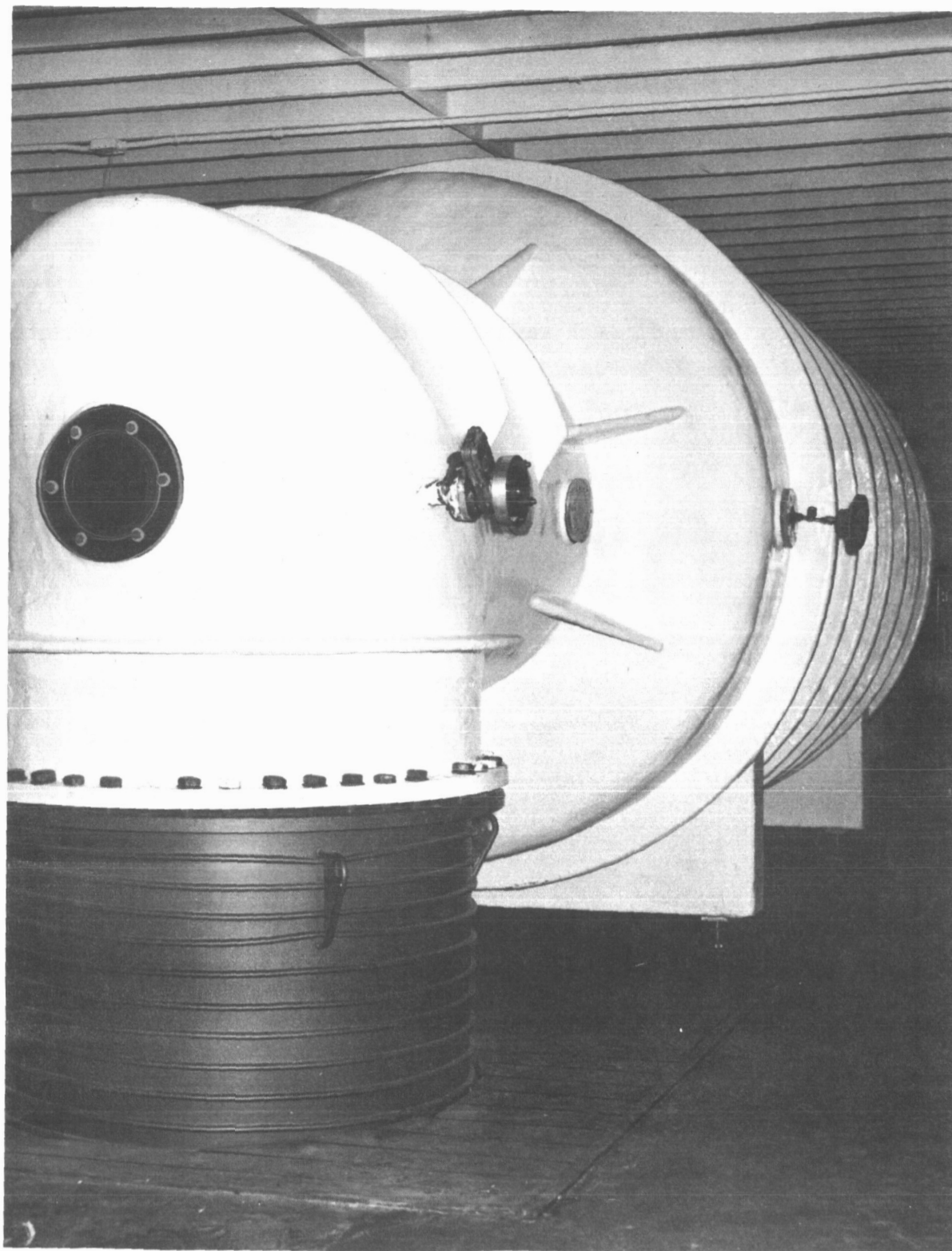
Figure 5.   Details of the Connections Between the Insulated Vacuum Tank
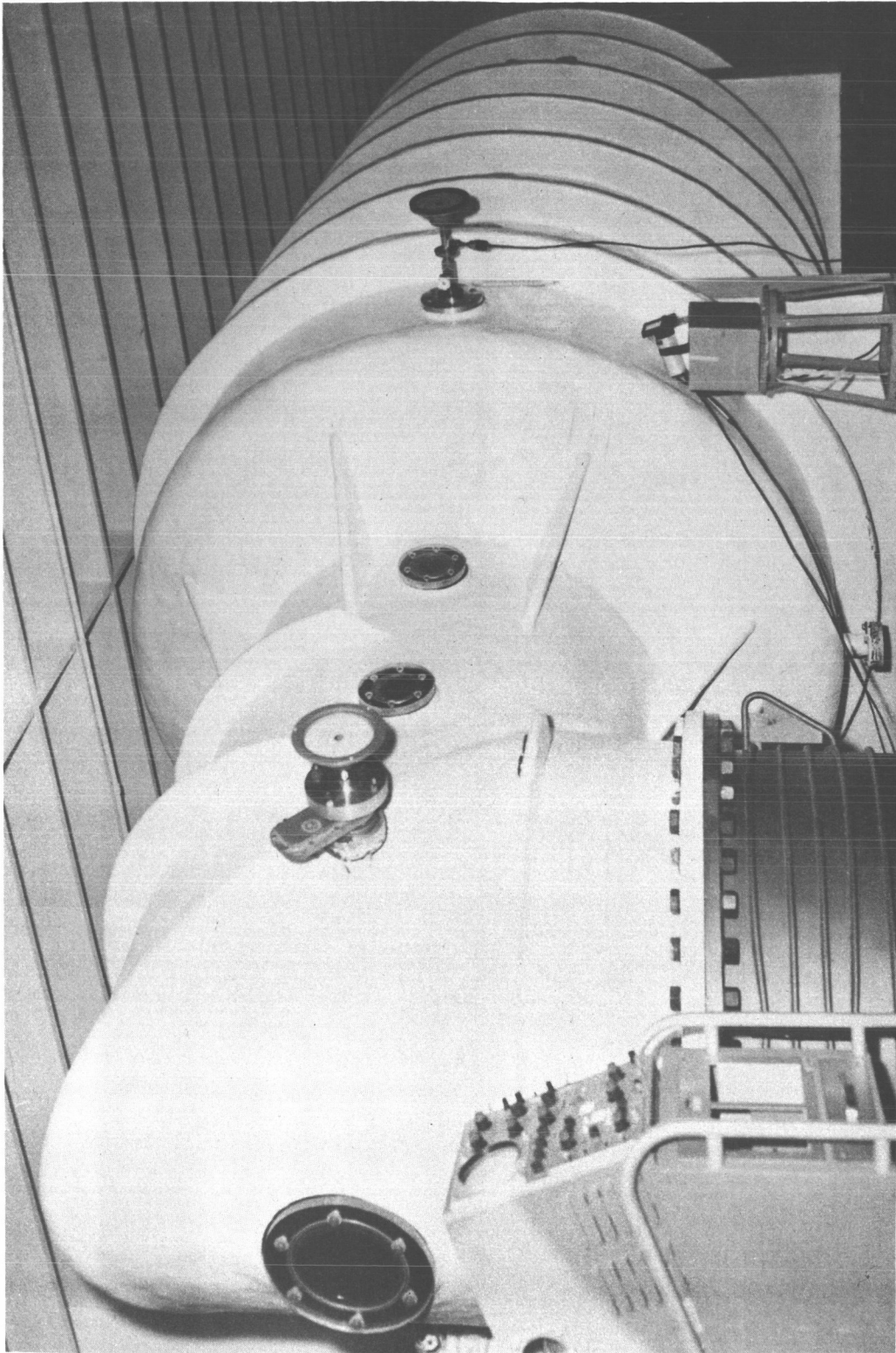and the 52-Inch Diffusion Pump

Figure 6. The Complete Vacuum Installation as Seen from the Diffusion Pump Side
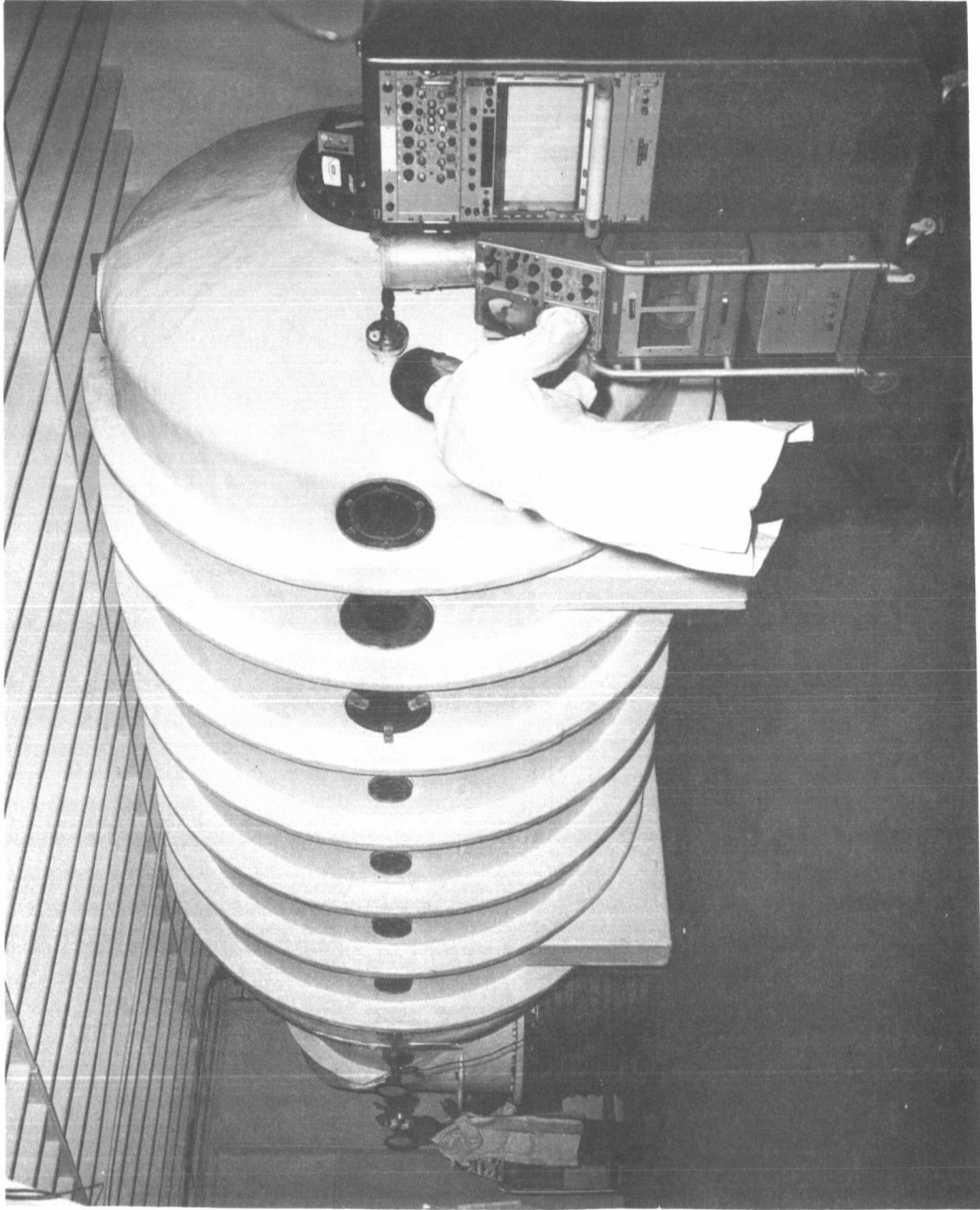
Figure 7. The Completed Vacuum System During Performance Tests

When the tank was completed a structural test was conducted before its transportation to our laboratory. A small mechanical vacuum pump was connected to the tank. Mechanical gauges applied between various points of the structure indicated a variation in length of 0.2 inch and a variation in diameter of 0.05 inch when the pressure was lowered from atmospheric to about half a torr -- variations that we consider perfectly tolerable and acceptable. At this point the tank was transported to its final location, lowered from the carrier to special low dollies and moved to its destination. A second vacuum test was then planned with a connection hose 4 inches in diameter to a 5000 cfm vacuum system using a blower and mechanical forepumps. The best vacuum attained after a period of operation of a few hours was about 20 millitorr. A small leak was suspected and finally localized as a microscopic crack near the bolts on one of the numerous windows. After repair a final vacuum pressure of 5.0 millitorr (using the mechanical vacuum pumps only) was recorded with a gradual decrease with the increase of the pumping time. It was noted that the lowest vacuum pressure was recorded in the early morning and the highest twelve hours later, suggesting an indirect effect of the daily temperature variations. After a certain period of pumping the minimum pressure reached in the vacuum tank using the 5000 cfm mechanical pumping system was under 3 millitorr. This pressure remained unvaried also during a prolonged pumping period suggesting the presence of a leak in the extended conduit system connected to the main mechanical pumping system. At this point a completely independent vacuum pump with a capacity of 1200 cfm was connected as directly as possible to the tank and after a nominal pumping period a vacuum pressure of about 2 millitorr was reached. This new pumping connection was activated day and night confirming that small variations in the vacuum pressure of the tank were dependent on the hour of the day and consequently on the ambient temperatures with a total variation from about 5 to 2 millitorr.

A measurement of the leak rate was attempted by closing the connection to the pump and measuring the consequent rate of increase of the vacuum pressure which was found to be dependent on the average pressure in the tank which, as mentioned above, was influenced by the daily variation of the ambient temperature. This behavior suggested that the rate of pressure building up when the pumping system was disconnected was not totally due to a leak but partially to evaporation of volatile materials inside the tank. For this reason the pumping was maintained uninterrupted for a full week obtaining a gradual improvement both in the pressure level and in the pressure buildup when the connection to the pumps was interrupted. It was found convenient to interrupt the pumping only for very short periods so as to avoid substantial variations in the tank pressure. A practical range adopted in the tests has been to measure the time elapsed to increase the tank pressure by only 0.1 millitorr. The best value obtained in this condition was an increase of pressure of about 0.5 millitorr per hour.

At this point the diffusion pump was activated both at low and high temperature of the silicone oil (type 704) and the evacuation continued uninterrupted during day and night for about 120

hours. The vacuum pressure was measured at various points of the tank with ionization gauges before and after cryogenic traps obtaining values which gradually improved with the pumping time. At the end of the period the lowest pressure measured in the tank without a cryogenic trap has been about 5×10^{-6} torr. With cryogenic traps and exactly at the same spots, pressures of about 5×10^{-7} torr have been measured. As determined when only the mechanical pumping system was used the value of the pressure was following the daily variation of the ambient temperature. The determination of the rate of increase of pressure in the tank with the pumping system disconnected (as done with the mechanical pump) has not been possible on account of the absence of a 52-inch valve in the diffusion pump inlet.

These tests and the preceding tests which were conducted with the mechanical pumping system, demonstrated that after the vacuum system has been exposed to the atmospheric pressure a long period of pumping is advisable before conducting any tests. For this reason it has been considered useful to develop a system which can maintain the insulating tank always at relatively high vacuum levels even when modifications in the experimental components are necessary. An important innovation that will be described later accomplishes this and permits an appreciable increase in the frequency of the tests, eliminating the long waiting periods during re-evacuation.

As soon as relatively high values of vacuum (very low pressures) were obtained a detailed research of residual leaks with the aid of a mass spectrometer has been conducted using helium and hydrogen as tracer gases. The results have not been satisfactory to date, the background signal level always being greater than the leak signal. By introducing calibrated leaks it has been found that as soon as a leak signal is obtained this signal persists for a long time after the artificial leak is removed, suggesting the trapping of traces of helium on the walls of the tank or in the oil of the diffusion pump. It seems necessary to develop different systems of leak detection if satisfactory results are to be obtained when using very large insulated tanks. As soon as satisfactory operating vacuum conditions have been reached a calibrated flow of hydrogen ranging from 0.05 to 2.0 mg/sec has been injected in the vacuum tank and the relative maximum pressures determined using ionization gauges connected directly to or after the cryogenic traps, as mentioned above. These results are shown in a condensed form in Table 1. Various interesting points are expressed in this table, as for example the net increase in pressure as soon as a small injection of external hydrogen is effectuated and the equalization of the "trapped" and "not trapped" pressure values when the injection is effectuated. This demonstrates that eventual minor leaks or evaporation in the insulating tank have practically no affect on the working pressure which is governed essentially by the amount of gas injected. The working conditions of the diffusion pump (when a continuous stream of propellant is injected in the vacuum tank) is to be taken into consideration in the design of the complete system. In particular, it has been found that most of the diffusion pumps on the market are designed to handle an amount of residual gases present in the system which is small compared to the amount of injected propellant. It is well-known

14

that the pumping speed of the modern diffusion pumps is practically constant from a pressure of 10^{-3} torr to the highest vacuum levels. However, a very important condition to be considered is the keeping of a certain forepressure level at the diffusion pump exhaust to avoid a deficient operation and excessive backstreaming of the evaporating oil. While a pressure around 100×10^{-3} torr is often indicated by manufacturers, we have found that a much lower forepressure is necessary to assure good operation when a continuous amount of external gas is injected. A forepressure has been selected of about 10×10^{-3} torr as a compromise between technical results and the cost of the system, and in particular to insure that backstreaming of the oil does not contaminate the tank environment. In the table the measured pressures are indicated for three different pumping systems; the first two columns are relative to a mechanical pump with a nominal capacity of 1200 cfm for air. The pressure values are divided into two columns; the first when a relatively long connection to the tank was used, the second with a direct connection. The great reduction in pumping speed in the first case demonstrates the necessity to locate the forepumps as near as possible to the diffusion pump outlet or to provide much larger diameter connecting pipes to reach the desired forepressure at the highest mass flow. Another fact demonstrated by these tests is a reduction of pumping speed in comparison to the nominal speed, especially at low values of flow and pressure.

If we consider, for example, a flow of 1 mg/sec of H_2 with a direct connection of the pumping system to tank (with a resulting pressure of 15 millitorr) the effective pumping speed is very similar to the nominal pumping speed (about 1200 cfm). But if this measurement is made at a flow of 0.1 mg/sec of H_2 always with a direct connection, the pumping speed is reduced (810 cfm). When a long connection is inserted between the forepump and the tank including the diffusion pump connection the pumping speed is reduced for the same two cases respectively to 240 and 144 cfm. The immediate consequence of this is the necessity to use forepumps with capacities much higher than the capacities conventionally recommended. Considering, for example, a maximum forepressure of 10 millitorr to obtain satisfactory operation of the diffusion pump the maximum H_2 flow (using a conventional 1200 cfm forepump) is about 0.5 mg/sec with a direct connection, but is reduced to 0.05 mg/sec if a long connection is used. Considering the third and fourth columns relative to a much more powerful forepumping system (5000 cfm nominal) the maximum flow using the same diffusion pump is augmented to about 2.0 mg/sec with a direct connection, but is reduced to 0.2 with a relatively long connection. This demonstrates that in designing vacuum systems to test under a continuous flow as is the case of propulsion the limiting factor for proper operation at a certain working pressure may not be the diffusion pump but can be the forepumping system and its installation. It is interesting to note that the recommended capacity of the forepump for our 52-inch diffusion pump is 250 cfm. As demonstrated before, to reach a value of the forepressure sufficiently low to reduce oil backstreaming and obtain satisfactory operation of the diffusion pump a much higher capacity of the forepump is needed. In the last two columns the effective pressures in the insulated tank, as measured with ionization gauges, are

TABLE 1

MEASURED TANK PRESSURE (TORR) WITH DIFFERENT FLOWS FOR THREE PUMPING SYSTEMS

Mass Flow mg/sec	1200 CFM Pump with Blower Connection to Tank		5000 CFM Pump with Blower Connection to Tank		140,000 liter/sec Diffusion Pump	
	Indirect	Direct	Indirect	Direct	measured with trap	measured without trap
0	1.5×10^{-3}	1.0×10^{-3}	4.7×10^{-3}	2.5×10^{-3}	0.5×10^{-6}	5.0×10^{-6}
0.01	2.0×10^{-3}	1.1×10^{-3}	5.0×10^{-3}	2.6×10^{-3}	1.0×10^{-6}	10.0×10^{-6}
0.05	7.2×10^{-3}	1.5×10^{-3}	6.8×10^{-3}	2.7×10^{-3}	2.3×10^{-6}	13.0×10^{-6}
0.10	13.0×10^{-3}	2.2×10^{-3}	8.2×10^{-3}	3.0×10^{-3}	4.0×10^{-6}	15.0×10^{-6}
0.20	21.0×10^{-3}	3.4×10^{-3}	10.0×10^{-3}	3.5×10^{-3}	8.0×10^{-6}	19.0×10^{-6}
0.40	35.0×10^{-3}	6.2×10^{-3}	14.0×10^{-3}	4.5×10^{-3}	17.0×10^{-6}	26.0×10^{-6}
0.50	42.0×10^{-3}	7.6×10^{-3}	16.0×10^{-3}	4.8×10^{-3}	20.0×10^{-6}	30.0×10^{-6}
0.80	58.0×10^{-3}	13.0×10^{-3}	22.0×10^{-3}	6.0×10^{-3}	31.0×10^{-6}	41.0×10^{-6}
1.00	70.0×10^{-3}	15.0×10^{-3}	25.0×10^{-3}	6.7×10^{-3}	38.0×10^{-6}	50.0×10^{-6}
1.60	100.0×10^{-3}	27.0×10^{-3}	33.0×10^{-3}	9.0×10^{-3}	70.0×10^{-6}	79.0×10^{-6}
2.00	$--- \times 10^{-3}$	35.0×10^{-3}	37.0×10^{-3}	10.0×10^{-3}	110.0×10^{-6}	100.0×10^{-6}
4.00	$--- \times 10^{-3}$	80.0×10^{-3}	59.0×10^{-3}	20.0×10^{-3}	$--- \times 10^{-6}$	$--- \times 10^{-6}$
9.00	$--- \times 10^{-3}$	$--- \times 10^{-3}$	105.0×10^{-3}	38.0×10^{-3}	$--- \times 10^{-6}$	$--- \times 10^{-6}$
10.00	$--- \times 10^{-3}$	$--- \times 10^{-3}$	$--- \times 10^{-3}$	50.0×10^{-3}	$--- \times 10^{-6}$	$--- \times 10^{-6}$

recorded. In the first columns the measurement is conducted through a cryogenic trap and in the second columns the measurement is direct. At the lowest pressures, differences of one order of magnitude are shown and this can be imputed to the presence of vapors or to a pumping effect in the gauge itself. It is interesting to note that at increased values of flow the difference between the two measurements gradually disappear and this might support the hypothesis that a small residual evaporation of the tank material is present at the lowest pressures. The relation between mass flow rate, pumping speed and tank pressure is illustrated graphically in Figure 17 on page 31 for a gas temperature of 0° C, and demonstrates the enormous pumping capacity required to reach very low tank pressures in case of a pumping efficiency of 100 percent.

In conclusion, during the first series of tests the insulating tank proved to be a satisfactory vacuum environment when more than 0.01 mg/sec mass flow was injected which makes the residual evaporation inconspicuous. The experience and know-how gained in this construction is considerable and should be very useful in the design of future tanks of much larger dimensions especially adapted for the direct connection to vacuum pumping systems of much higher capacity. This possibility is important in our opinion for the testing of higher power thrusters of any type in a relatively high vacuum and without an undetermined interference of tank walls. With the tank and vacuum system just described it is anticipated that regular tests can be conducted with mass flows ranging from a fraction of a milligram per second to several milligrams per second in an environmental vacuum pressure ranging from 10^{-6} to 10^{-3} torr. An important point demonstrated by these experiments is that in regular use an insulating vacuum tank is more versatile than a metal tank and perhaps more economical.

2.2   Construction of a New Thrust Stand

It is common practice to support the thruster in the vacuum chamber with a force measuring system which is called generically a "thrust stand." The thrust stand is normally located in the extreme part of the vacuum chamber (opposed to the pump inlet) and contains thrust measuring accessories together with the terminations of all the connections to the thrusters. These are electrical and mechanical connections of a varied nature such as cables, hoses, etc. After long experience in the operation of thrust stands of various characteristics and the analysis of their behavior, we became suspicious that the presence of the thrust stand in the vacuum chamber was contributing to errors in the measurement of thrust. The reasons for this attitude are as follows: The presence of a highly ionized atmosphere around the jet permits the formation of current paths between conductors present in the vacuum tank. The condition may produce secondary dynamic effects that can influence the thrust readings. In our past experiments strong discharges have been produced between conductors located at a relatively large distance from the jet as illustrated in Figure 8 and appreciable currents along the metal tank walls have been suspected. Hence, during the last year
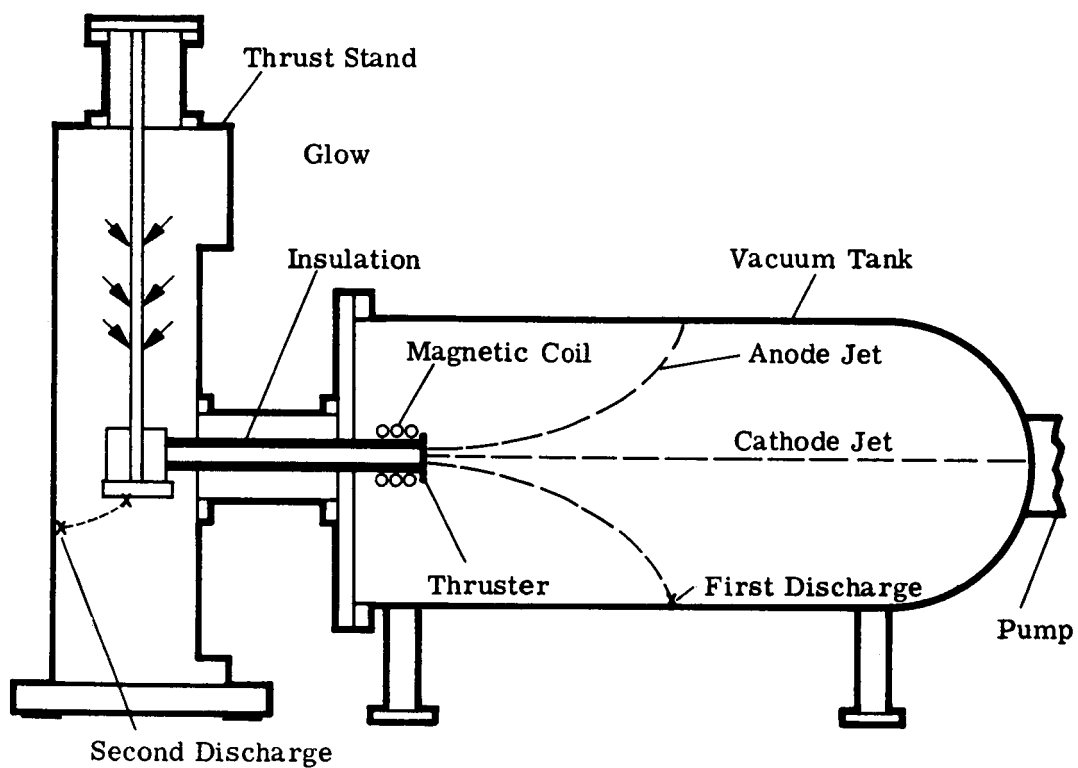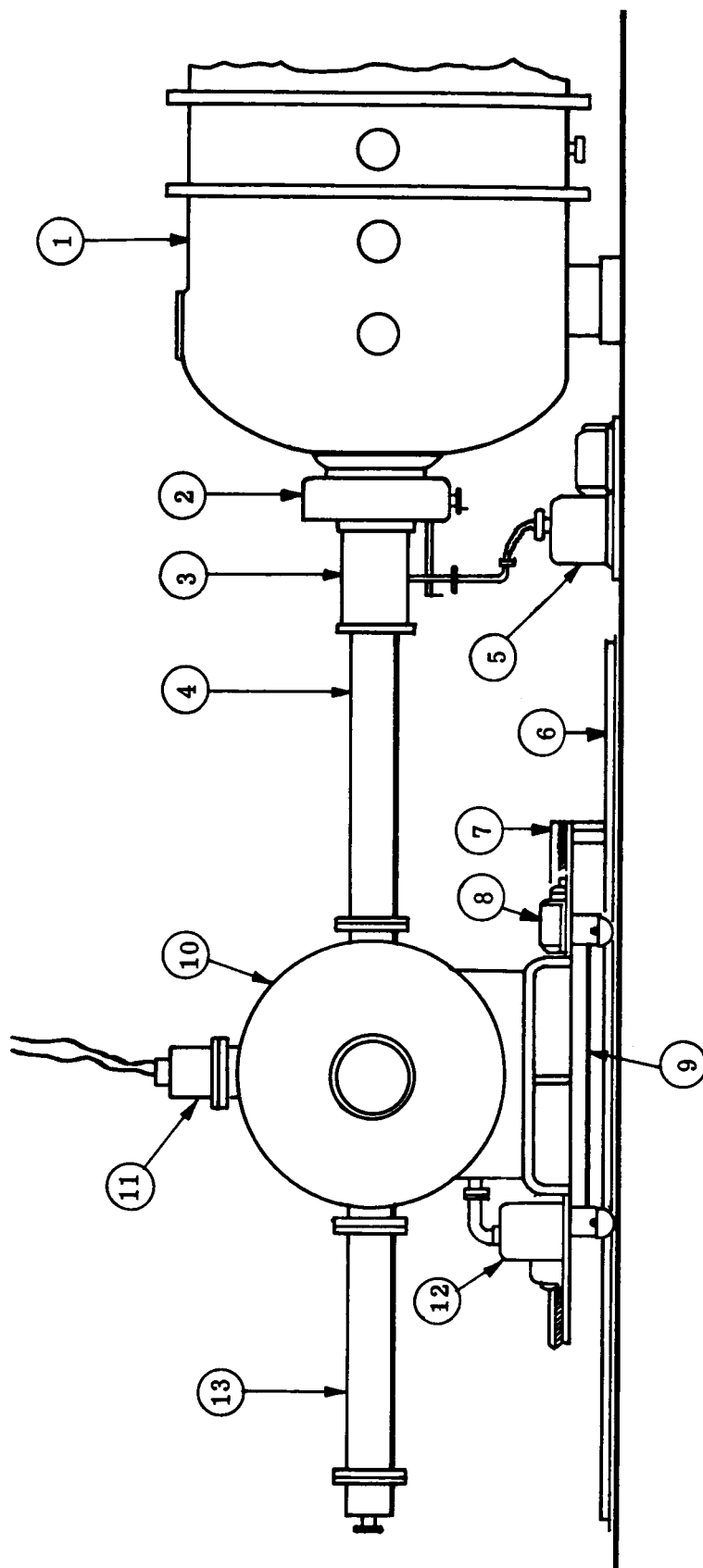
Figure 8. Schematic of Earlier Facility Illustrating Discharges
to the Metal Vacuum Tank

our thrust stands have been designed to be separated from the vacuum chamber and connected to it only through an open pipe of small diameter. This partial separation reduces the possibility of discharges in the ionized atmosphere around the thruster, especially when relatively small external magnetic fields were used. However, increasing the external magnetic field increases the protrusion of the arc current into the vacuum chamber and may cause a higher level of ionization in the atmosphere surrounding the thrust stand, and an increase of parasitic current paths. In a very recent series of experiments[2] it has been found that another source of interference is possible when the thrust stand is located in the vacuum chamber. It appears that on account of the displacement of residual gases flowing between the various zones of the vacuum chamber under a combined sucking action of the plasma jet and the pump, substantial aerodynamic forces originating within the tank could be present. These forces might act directly on the thrust stand if it is located in the vacuum chamber, producing erroneous thrust values. For these reasons, i. e., production of parasitic electrodynamic effects from spurious electrical currents in the vacuum tank and the production of parasitic aerodynamic effects by circulating gas currents due to the pumping effect of the plasma jet, a new approach for the location of the thrust stand appeared necessary. The complete mechanical and electrical isolation of the thrust stand from the vacuum chamber has been put into effect. The isolation of the thrust stand has been accomplished in the manner shown schematically in Figure 9 and in more detail in Figure 10. The particular construction of the thrust stand, which has been developed to meet the exacting requirements of low thrust measurements, is also convenient for another important step in the experimental procedure. As pointed out above, the high vacuum levels in the chamber are relatively easy to maintain as soon as a certain vacuum level is reached, but require a long period of evacuation if atmospheric conditions are to be overcome as happens when the vacuum chamber is opened between tests for the interchange of thruster components. The ideal solution is to keep a permanent high vacuum in the testing chamber even when tests are not being conducted. This can be done with a small permanently connected diffusion pump. In this case it is only necessary to install a secondary vacuum prechamber, which can be slightly larger than the thruster, right at the entrance of the tubular termination of the thrust stand as shown in Figure 10. This secondary chamber can be easily evacuated with a subsidiary vacuum pump. When pressure equalization with the principal vacuum chamber is obtained, the separating vacuum valve is opened and the thruster is inserted in the tank. A 5-inch inside diameter vacuum valve is needed to permit the passage of the thrust stand tubing; this type of valve is easily found on the market. However, to maintain a totally insulated environment a similar valve has been constructed in our shop using exclusively insulating parts as illustrated in Figure 11. During the operation of the thruster this valve remains completely open and is closed only when the thruster and its thrust stand is retracted. An auxiliary vacuum must be applied at the opposite side of the main tank any time the valve must be operated not only to permit an easy slide of the gate, but also to avoid the introduction of a slug of high pressure air inside the evacuated tank. If the tank is evacuated to a pressure of 10^{-5} torr a difference of one order of magnitude in the pressure at

Figure 9. Schematic of Vacuum Test Facility Showing Isolated Position of Thrust Stand from Vacuum Tank

1. Fiberglass vacuum tank
2. Plastic vacuum gate valve
3. Insulated bearing and prevacuum chamber
4. Insulated thruster arm housing
5. Prechamber vacuum pump
6. Guiding rail
7. Driving rack
8. Electric motor with gear drive
9. Thrust stand supporting frame
10. Thrust stand housing
11. Feed line connecting housing
12. Thrust stand vacuum pump
13. Thrust stand balancing arm housing

Figure 10. Schematic of Retractable Thrust Stand

1. Thrust balance arm
2. Balance arm housing
3. Vacuum manifold
4. Vacuum gate valve
5. Precision flex-joints
6. Balance arm joint
7. Feed line housing
8. Thrust micro balance
9. Thrust stand housing
10. Solenoid bleed valve
11. Thruster arm housing
12. Prevacuum chamber
13. Vacuum gate valve
14. Insulated face plate
15. Fiberglass tank
16. Magnetic field coil
17. MPD arc thruster
18. End cap
19. Diaphragm
20. Thruster arm
21. Prevacuum pump
22. Vacuum manifold
23. Driving rack
24. Drive motor
25. Thrust readout transformer
26. Low friction casters
27. Supporting frame
28. Locking arm
29. Locking mechanism
30. Vacuum forepump
31. Diffusion pump
32. Guiding Rail
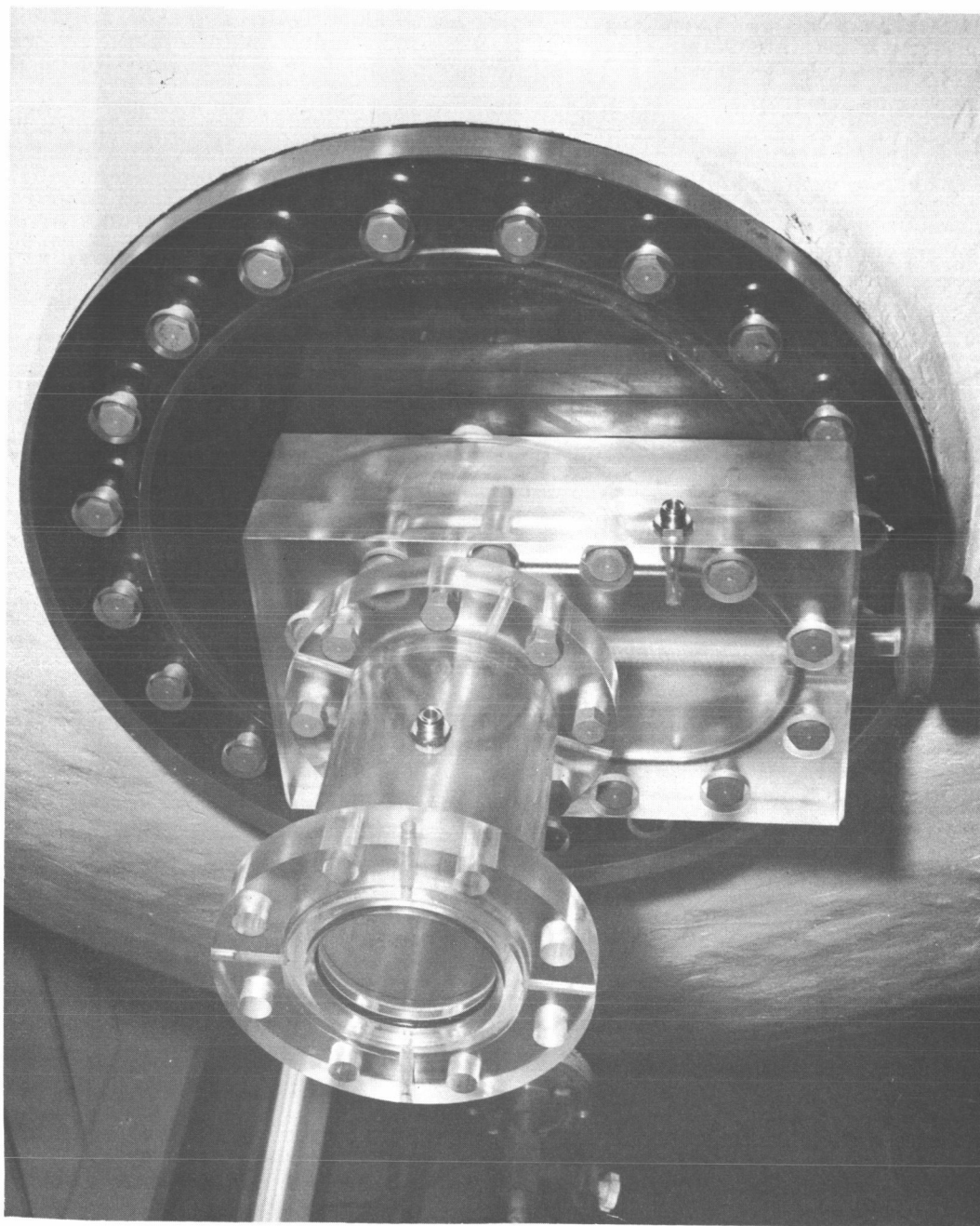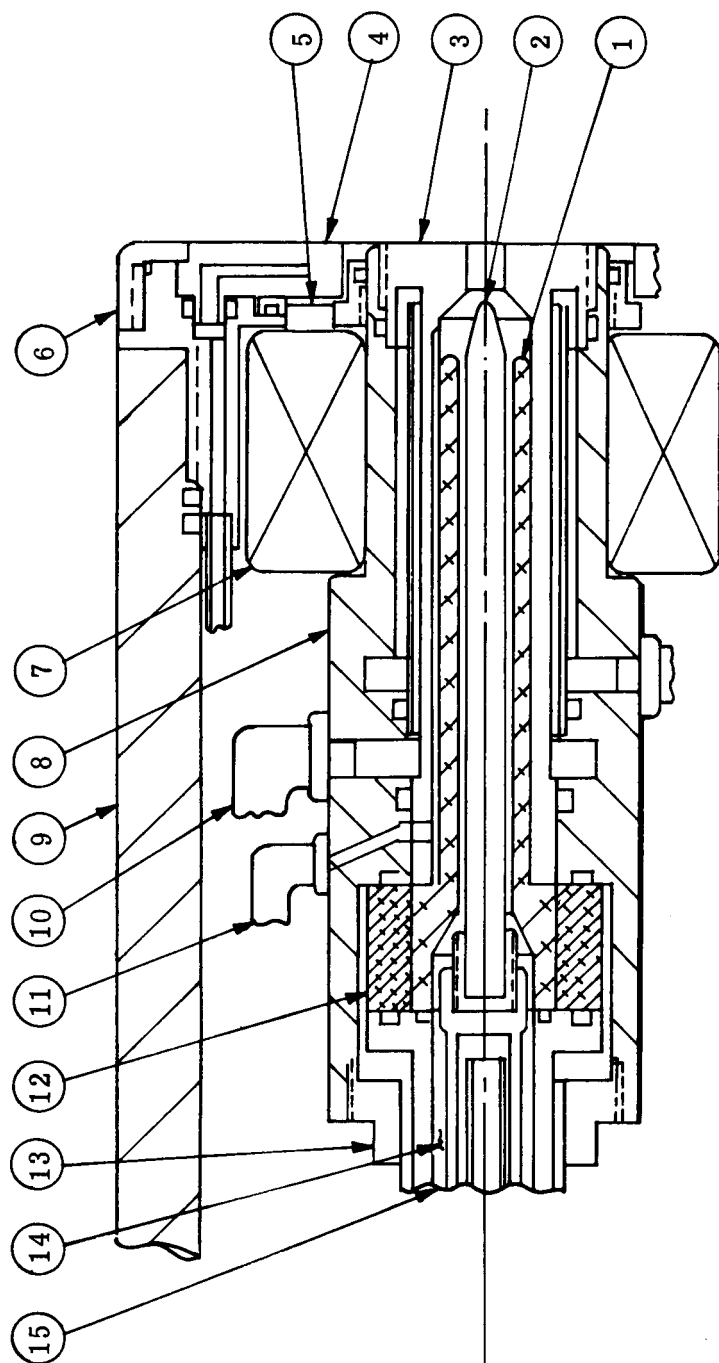
Figure 11. Photograph Showing Installation of Plastic Vacuum Gate Valve to Fiberglass Tank

the opposite side of the valve is hardly detected. During a series of routine tests this system of operation proved to be very fast and efficient and the total time required to exchange the thruster parts has been reduced from a few hours at best to a few minutes in most of the experiments.

To reduce to the minimum the intervals between the tests it is not only necessary to use the above described double vacuum chamber system, but also it is important to design a thruster whose parts are rapidly and easily interchanged. The complexity of the internal connections both electrical and mechanical and the relative long time required for their final setup, makes it imperative that any exchange be effectuated from the front of the thrust stand. For the completion of the programmed tests various geometries of electrodes are contemplated, each one different from the other by diameter and length with a total of about 16 anodes and 16 cathodes. It has been decided that the "base" of the thruster will be so designed to receive with a fast connect system and with complete interchangeability all these electrodes. This type of construction is illustrated in Figure 12. It is estimated that the above-mentioned 16 pairs of electrodes will be interchanged more than ten times each during the total test period for substitution or modification bringing the total interruptions of the test to around 200. It is evident that the reduction of the time necessary for this operation has a very important influence on the final results. For each geometry variation the most important operative parameters of the arc jet will be varied, as for example the intensity of the magnetic field, the mass flow and the power input. This variation will not require any change of electrodes except substitution when life limits will be reached. Considering an average repetition of three times for each condition, the anticipated total number of tests will be very large. For this reason the conduction of the tests must be planned in advance as done in a regular production line with minimization of any idle period and with the most efficient sequence of the various operations. Changing the mass flow as contemplated in the program will automatically change the vacuum chamber pressure which will be minimum for the smallest mass flow. To obtain comparable results it may be necessary to inject in the vacuum tank (externally to the thruster) a certain amount of propellant to maintain a constant tank pressure at any mass flow. In this case it will be advisable, especially for the extremely small mass flow, to repeat the test both at constant and at minimum pressure. This will increase the total number of tests to be conducted.

The picture of Figure 13 shows the same thrust stand as it appears when connected to the insulated vacuum chamber. A thin insulating membrane separates the thrust stand from the vacuum chamber as illustrated in Figure 10 and two completely separated vacuum pumping systems are used in the two different environments. The pressure in the two compartments is maintained exactly at the same level so the two atmospheres are balanced and no dynamic effects are present between them. The small area of the separating membrane and the low operating pressure assures that small differences in pressure between the two environments can have no affect on the thrust reading. (It is also anticipated that small calibrated differences in pressure might be used to balance the thrust operating constantly at zero reading.)

Figure 12. Design of 10 kw Water-Cooled MPD Arc Thruster Which Permits Fast Interchange of Electrodes

1. Insulator (rapid interchangeable)
2. Cathode (rapid interchangeable)
3. Anode (rapid interchangeable)
4. Front shield (water-cooled)
5. Flexible diaphragm
6. End cap
7. External magnetic field coil
8. Anode housing
9. Insulated thruster arm housing
10. Cooling water inlet
11. Arc chamber pressure tap
12. Insulator
13. Lock nut
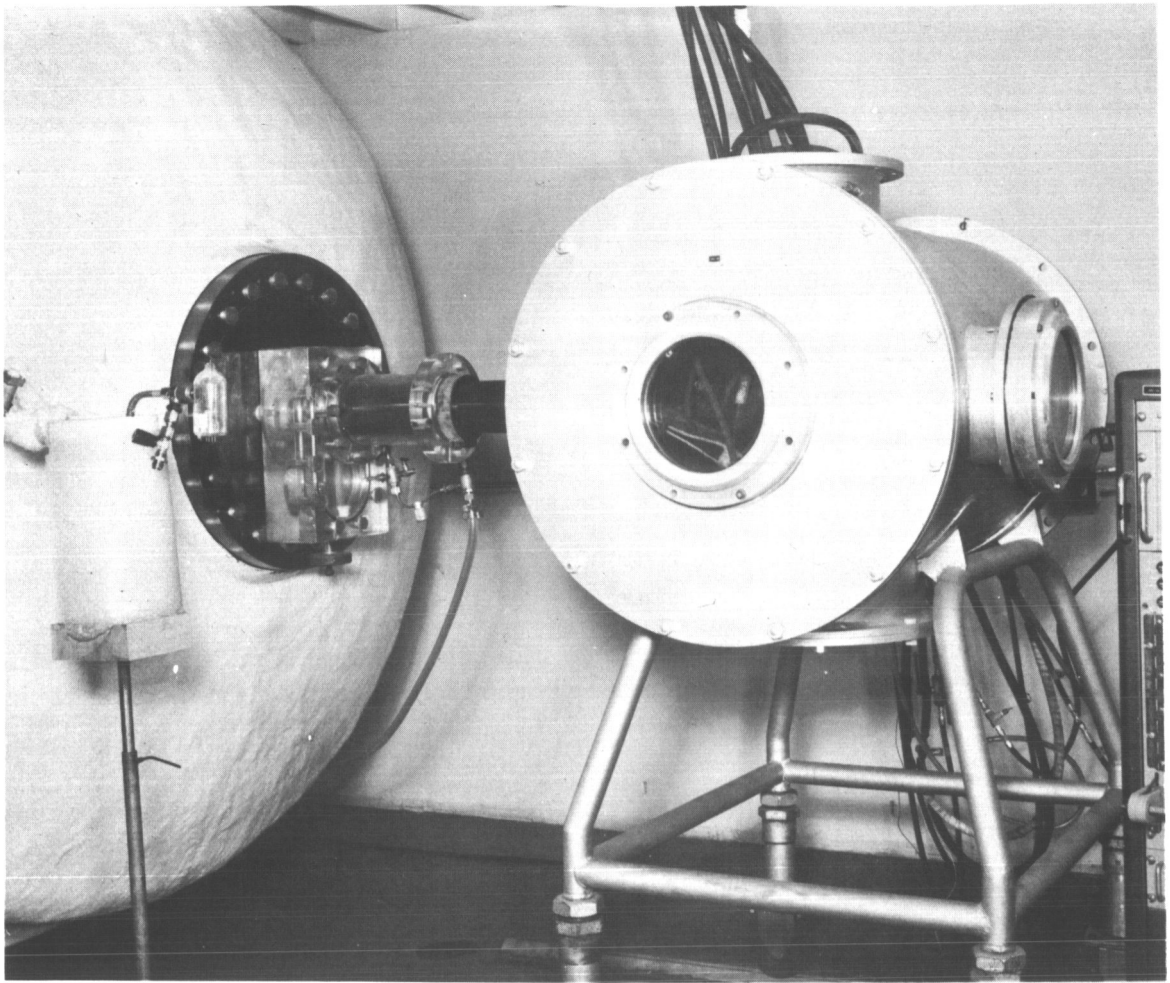14. Propellant injection passage
15. Cathode housing

23

Figure 13. Photograph of Thrust Stand Housing Connected to Fiberglass Tank

2.3   Preliminary Tests

Tests were conducted in order to obtain information to aid in the design of the insulating vacuum tank, to determine the materials to be used in its construction and to establish suitable dimensions for the tank. An investigation of the feasibility of constructing a glass tank was carried out and showed that it was not possible to construct a completely glass tank exceeding two feet in diameter, while using separate glass sectors with intermediate rubber sealing gaskets between the various elements it was not possible to obtain diameters larger than four feet. In conjunction with this study a regular metallic vacuum tank was lined with a two foot cylinder of insulating material. Tests conducted in this environment with a thruster operating at relatively high specific impulse and intense magnetic fields showed strong heating of the walls and circulating gas currents along the insulating walls. These results suggested that it would be desirable to have tank diameters exceeding four feet which ruled out the glass tank which was initially proposed. The study was then directed toward the use of plastic materials with special attention to a fiberglass material which is employed with success in the construction of tanks of large dimensions used especially for the storage and transportation of liquids. Since tanks of this type of material have not previously been used for steady thruster operation,[3] we considered it advisable to first test a scaled-down model. A tank about 1/100 of the final dimensions was constructed and tested under vacuum and high temperature so as to determine its vacuum characteristics. Tests conducted on this miniature tank were sufficiently encouraging to proceed with the design of a 10 x 25 foot tank along identical lines using the same plastic materials which were used in the miniature tank.

A series of tests were conducted in the metal tank with the insulating lining to determine the temperature and power distribution to the tank walls to be expected in the fiberglass tank. Thermocouples distributed along the internal surface of the insulating lining were used to determine the wall temperature as a function of the thruster operating conditions. A series of calorimeters distributed along the insulating cylinder were used to determine the distribution of the power load to the wall. The calorimeter measurements showed a relatively sharp maximum in the power transferred to the wall at about ten inches from the face of the thruster, while at an axial distance of four feet from the thruster essentially all the power in the gas has been transferred to the tank walls.

During the construction of the insulating tank a long series of tests were conducted to determine the best working conditions for the high capacity diffusion pump used with the insulating tank. A special steel plate was constructed to seal the upper flange of the pump already assembled in its final position. The possibility for interconnecting two different forepump systems have been provided. These are distinct pumps having a capacity of 250 and 5000 cfm for air respectively. During this series of tests the best vacuum obtained has been about 1×10^{-7} torr measured at the center of the top plate of the diffusion pump

with a trapped ionization gauge. The leakage of the completely installed pump including the connections to the various forepumps produced a pressure rise of a few millitorr every 24 hours.

While these tests were being conducted the development of the new very sensitive thrust stand already described in this report was initiated. On account of the relatively small mass flow admitted by the limited pumping capacity available (1.4×10^5 liter/sec) the thrust measuring system must be able to determine a 10 milligram force and this is a sensitivity already equivalent to that of a laboratory scale. Some preliminary tests which may be applied to the design of the thrust stand to be used in the final tests show a sensitivity of about 10 milligrams per division and this permits us to forecast that a similar sensitivity will be obtained when the completed thrust stand will be operated in the vacuum chamber.

A thruster has been operated in the new tank with a 1 mg/sec hydrogen flow rate. The ambient pressure near the pump with the arc running was the same as it was with an equal cold hydrogen flow rate.* Hence, there is so far no indication that increased outgasing due to the arc discharge or the plasma jet is going to increase the ambient pressure. However, the arc has been operated continuously only for short periods of time. The thruster which has been operated in the new tank is similar to the 5 kw thruster developed here in 1965 to test the effect of scaling on performance.[4] The design and performance of this thruster is given in Reference 4. During future tests we will compare the performance data which was obtained in a metal tank with the performance in the larger insulated tank.

The following discussion is based on measurements in the series of tests in the new tank which have just been initiated. We find that the arc runs in a stable mode over a considerable range of magnetic field strengths at a total arc power in the neighborhood of 8 kw. We are using 1.0 mg/sec mass flow rate so these are very high specific enthalpy jets. We do not anticipate any difficulties in obtaining stable operation over a range of arc parameter values comparable to that which is possible in the higher mass flow arcs operating at higher ambient pressures in a metal tank.

The visual appearance of these high power density flows is different in some respects from the arcs operating in the metal tank at higher pressure[4] (see Figure 14). There is a bell-shaped plume near the thruster with a bright axial core as shown in Figure 15. However, the central luminous region emanating from the cathode tip is greatly exaggerated, extending way out from the thruster and then turning toward the tank wall as shown in the color photograph. The luminous streak does not end at the tank wall as it appears to do in Figure 16; this is just the first quarter turn of a huge variable pitch spiral that extends much further down the tank and is sometimes clearly visible to the eye. Part of the first turn of the

---

*The ambient pressure may not be the same at different positions in the regions of the tank outside the plume. The pressure in a smaller metal tank at higher ambient pressures has been found to be highest at the pump end of the tank.[2]
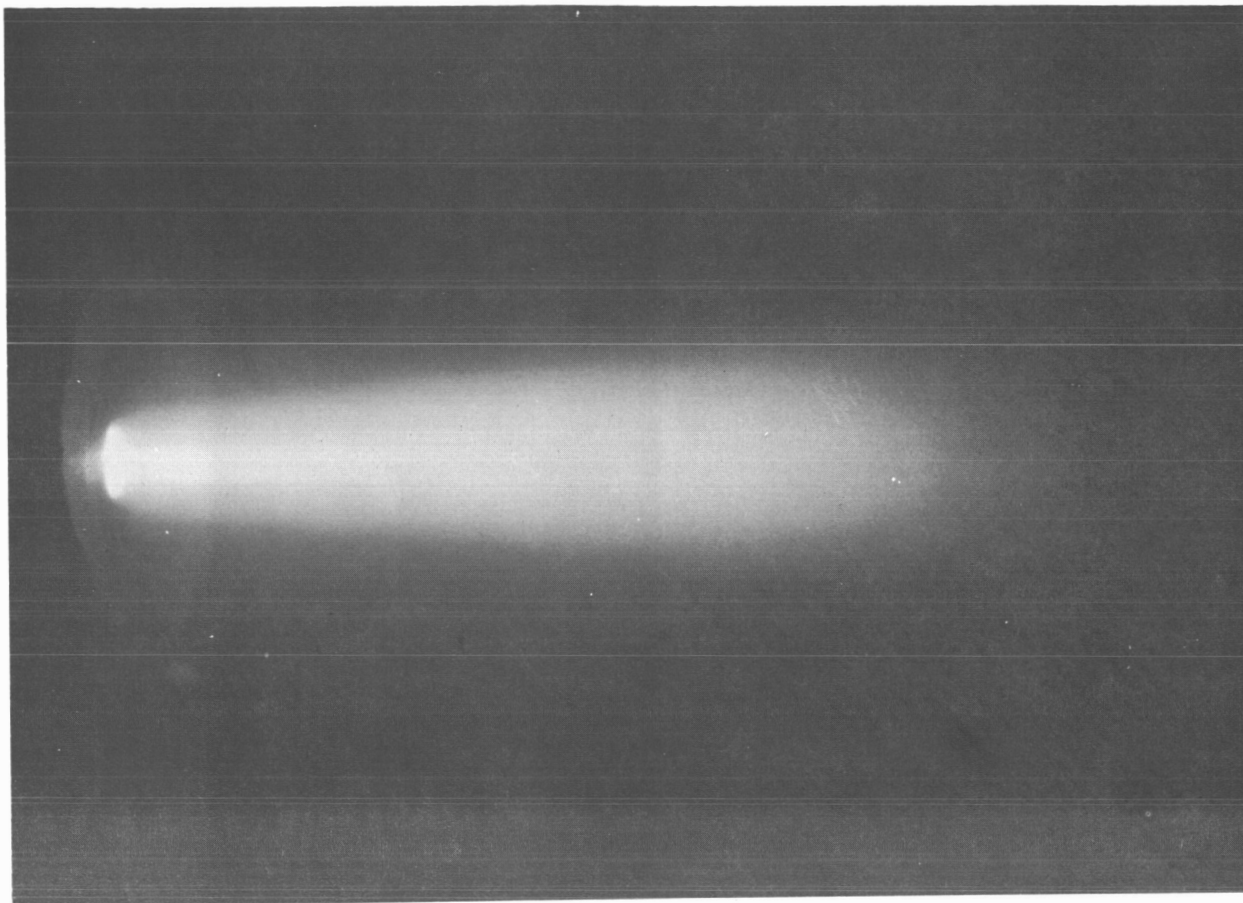
Figure 14.   5 KW Thermo-Ionic Thruster in Operation (H_2 Propellant)

Figure 15

Photograph showing extended cathodic discharge first turning toward the
tank wall and then back toward the center of the tank. The sharp bend in
the discharge occurs about four feet from the thruster face.
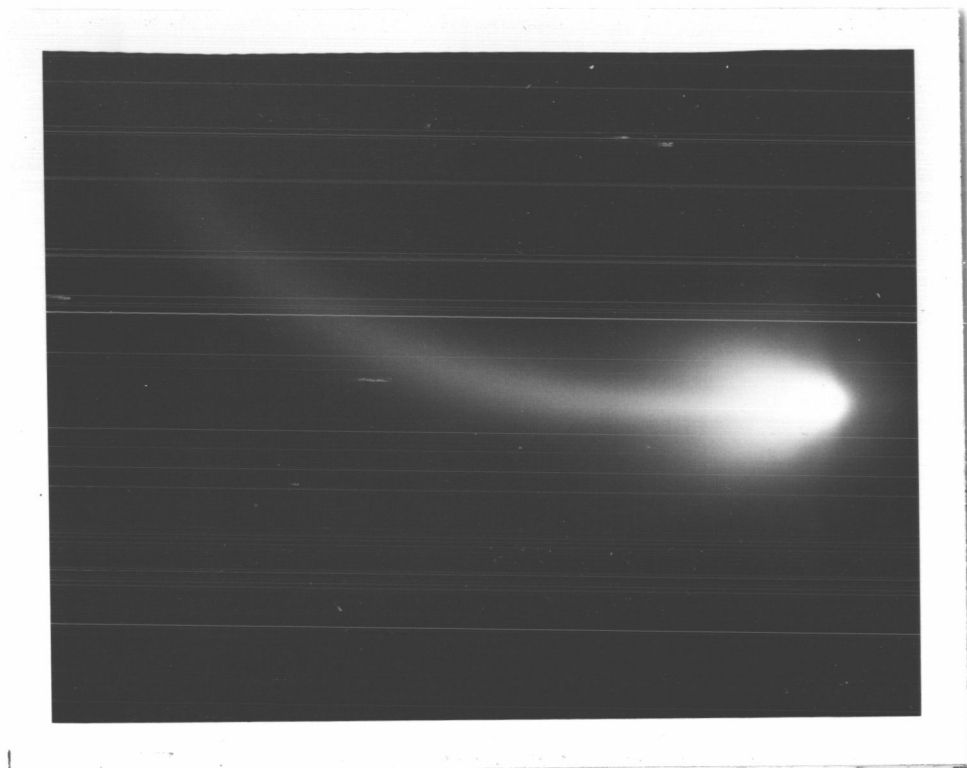
Figure 16

Photograph of extended cathodic discharge and plume in the fiberglass tank at 4×10^{-5} torr ambient pressure, 1 mg/sec hydrogen mass flow, 8 kw arc power, and 2 kilogauss applied magnetic field.

spiral can be seen at the left side of the photograph in Figure 16. The first turn of the luminous streak takes place near the tank wall and grazes the wall in a manner that produces a slight burn there. When a magnet is placed near the luminous spiral it moves, which shows that the spiral carries current. If the direction of the coil current is reversed, the sense of the spiraling also reverses. When the magnetic field is increased, the extended luminous region becomes less distinct and for strong magnetic fields the clear separation of the discharge and plume into separate regions tends to disappear and the plume acquires a more uniform diffuse appearance.

The arc voltage has been measured as a function of magnetic field strength and in the few tests that have been made we have found slight differences in the usual increase of the voltage with magnetic field. Probably the peculiar appearance of the arc and the voltage characteristics are related. It is presently not clear what is responsible for the different voltage characteristic or extended cathodic discharge and what contribution to the thrust is associated with it. We presently feel that it is an inefficient mode of operation and that a more desirable condition of operation must be found. A complete account of the performance and arc characteristics in the low pressure insulating environment will be presented after a series of tests planned for the continued program are completed.

Figure 17. Vacuum Pressure at 0° C as a Function of Mass Flow Rate and Pumping Speed

This graph shows the pumping speed in liter/sec for hydrogen mass flows in the range of 0.01 to 10 mg/sec required to obtain a desired tank pressure at 0° C. The scales are to be read in the diagonal direction with the arrows indicating the direction of increase of pressure, pump speed and mass flow. The graph illustrates the large pump speeds required to obtain very low tank pressures. For example, we see from the graph that to obtain 10^{-6} torr tank pressure at 1 mg/sec mass flow rate, a pump speed of 8.6×10^6 liter/sec is required.

MASS FLOW RATE, MG/SEC

10.

1.

.1

.01

1

10⁻¹ 10⁻² 10 10² 31-B

10^{-3}

10^{-4}
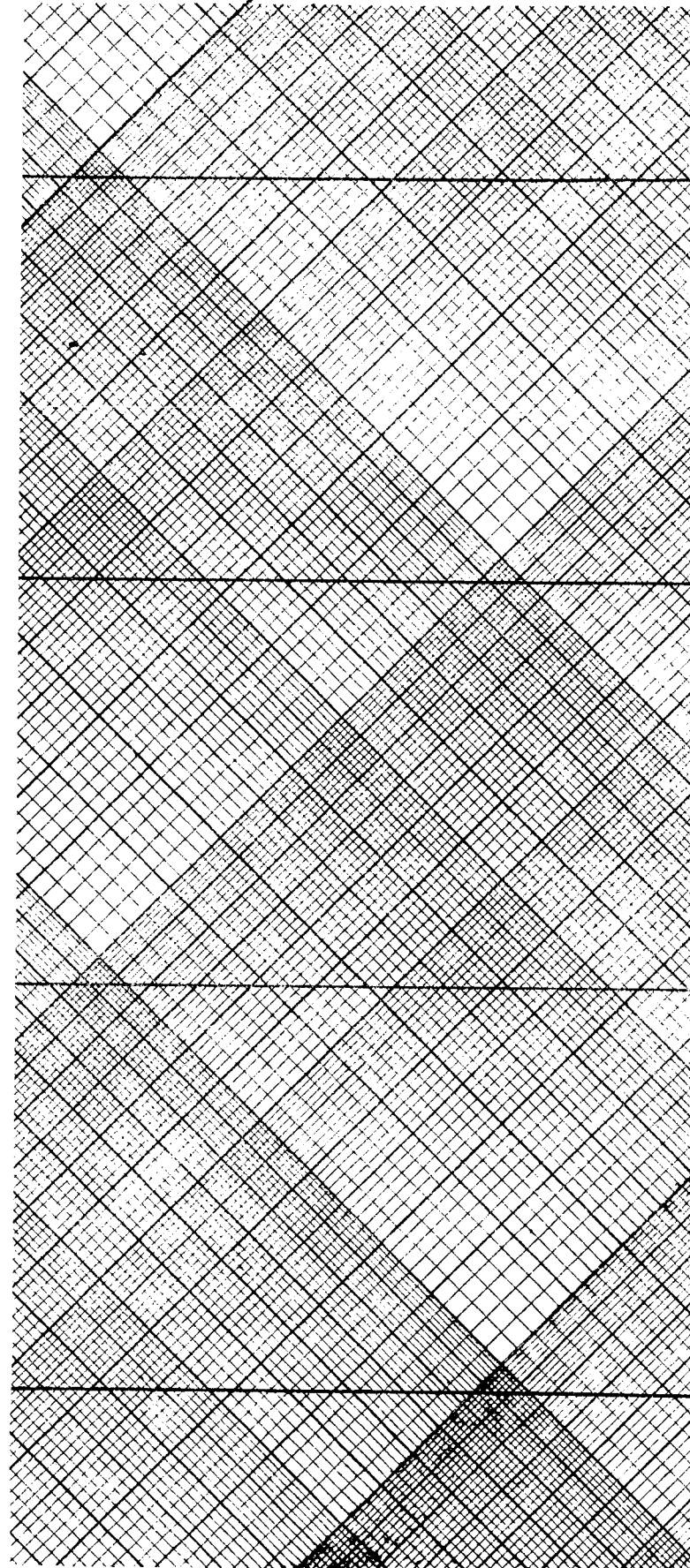
FOLDOUT FRAME 10^4 LITER/SEC

10-5

10-6

10 5

10 6

31- D

10-7

10-8

Figure 17

10^7
31-E

10^8
31-F

PRECEDING PAGE BLANK NOT FILMED.
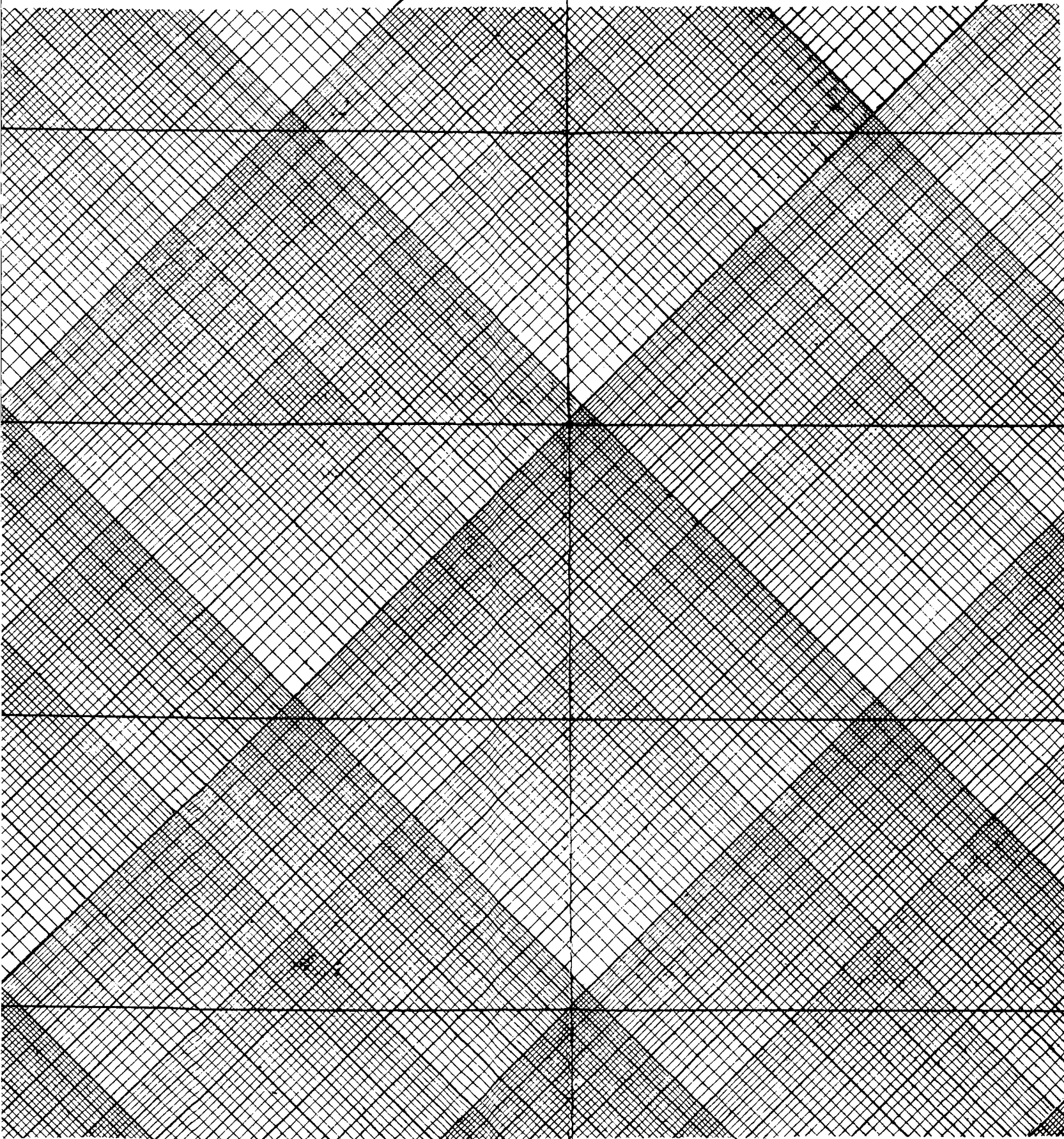
3.0 THEORY

3.1   The MPD Arc: to $\vec{B}$ or Not to $\vec{B}$, ... , by Robert G. Jahn

3.1.1   History

Development of the coaxial arc jet for plasma acceleration has been primarily an empirical process, and the accumulated bulk of terminal performance data far outweighs any detailed understanding of the physical mechanisms prevailing in such devices. While perhaps justifiable on the basis of the complexity of the phenomena, the multivaried significant parameters, and the urgency of application in several technologies, this empiricism, unless regularly supplemented by incisive research, can lead to entrenchment of inferior techniques on no firmer basis than simple familiarity or local convenience. One technique requiring such basic re-examination is the use of external magnetic fields to improve arc jet performance for propulsion.

Long before the arc jet graduated into its high performance or MPD mode -- indeed, even before it had any propulsion aspirations -- it was casual common practice to add a few turns of current lead around the arc head to provide a modest axial bias field which kept the anode attachment from localizing and melting the electrode. With the dis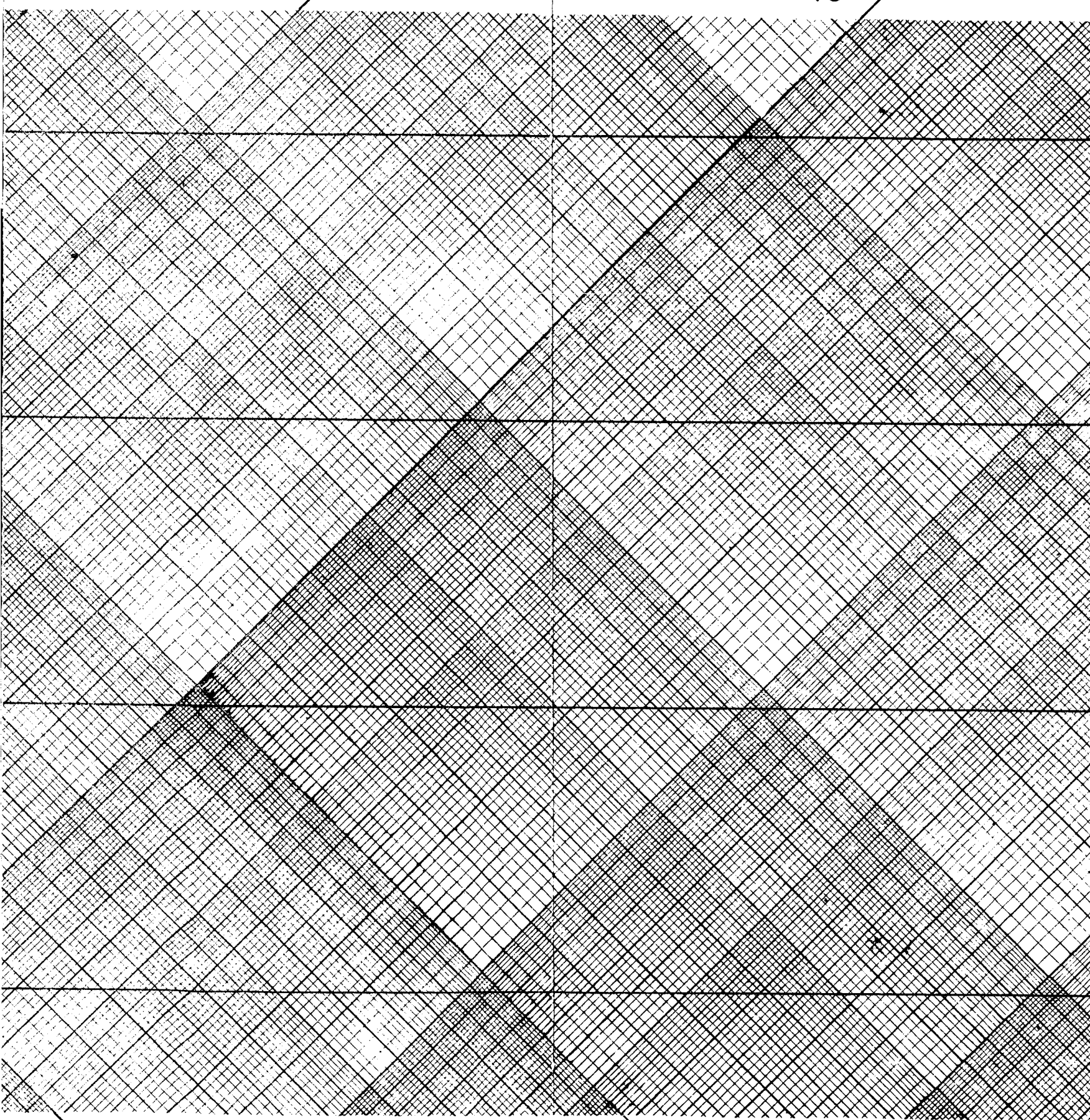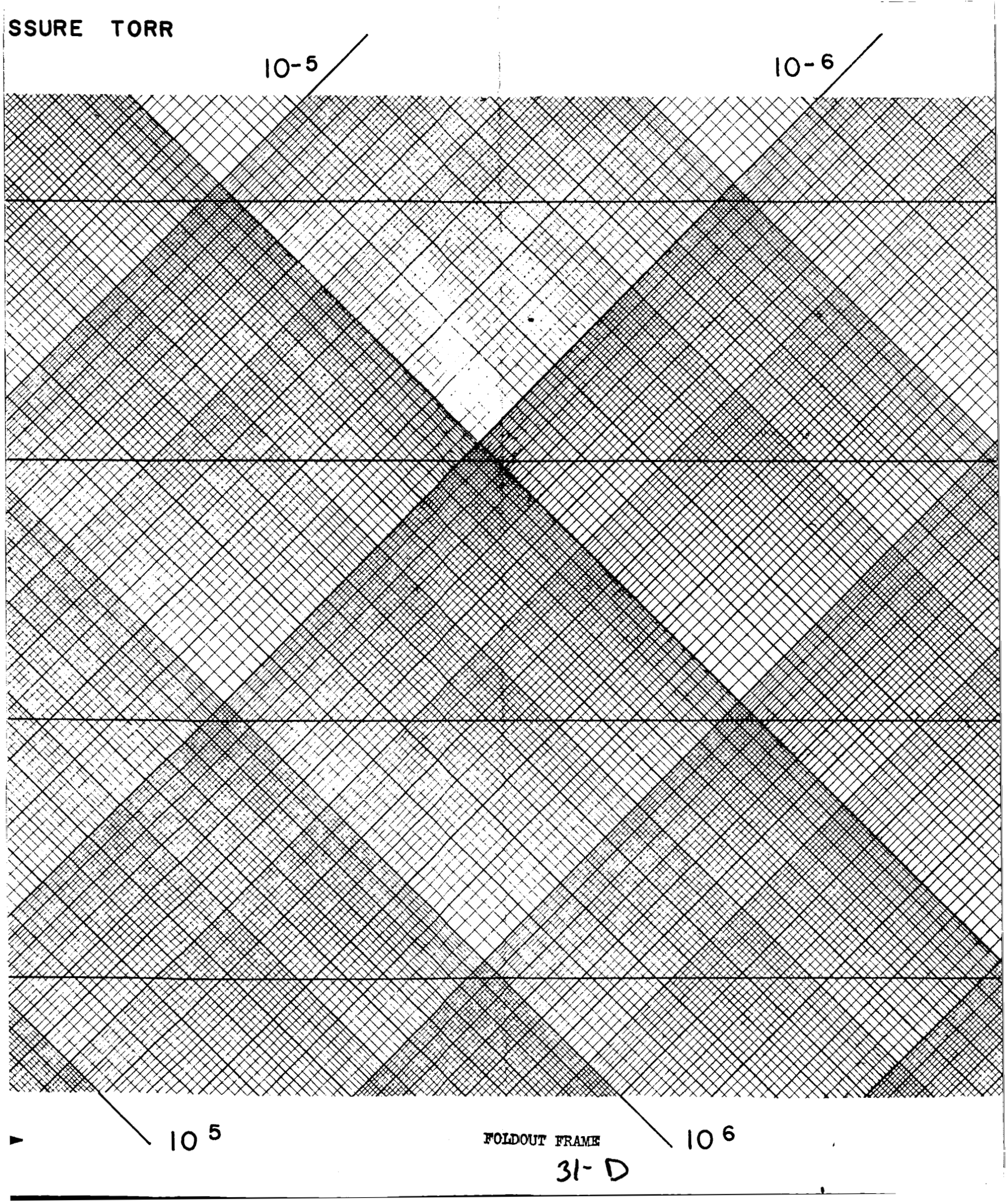covery of the high current MPD capability, and the subsequent preoccupation with long-life operation, protection of the electrodes became a more primary concern. Initially it seemed that high current discharges at low pressures in this geometry might be inherently diffuse and azimuthally uniform, but a variety of long-life tests indicated either a tendency to gradual localization and subsequent ablation of a portion of the anode or a more abrupt and devastating spontaneous transition to a spoked mode at random and unpredictable times during the test. In either case, remedy was again empirically provided by a modest axial bias, and the testing programs continued without detailed evaluation of the interaction of this field with the discharge plasma.

In the course of adjusting the strength and configuration of the applied field for minimum erosion, other effects were also noted: With increasing field, the exhaust plume first constricted radially and extruded axially, and later developed a well-defined shell-like structure of "cathode jet" and "anode jet." For fixed current, the arc voltage increased with increasing bias, the arc chamber pressure increased, but the cathode tip pressure decreased.[5, 6] A new component of thrust could be identified, roughly proportional to the product of arc current and bias field, and this encouraged a return of those interested in low power thrusters to the concept of the so-called coaxial "Hall current" accelerator, where the external field was intended to provide the major portion of the thrust. At present there is considerably more effort spent on these devices than on the higher power, self-field

33

accelerators which first excited the MPD program, but even here, understanding of the details of the field-arc interaction is rather superficial.

Regardless of the particular power range of immediate interest, it now seems worthwhile to re-examine more critically the role of the external field in an MPD arc, first because of its explicit and implicit contributions to the specific mass of a propulsion system from coil weight, added demands on the power plant, and heat dissipation, and second because of possible inherent disadvantages to optimum arc operation. The proposed task will be difficult for two reasons: first, there are many permutations of prevailing conditions to be considered; and second, certain critical experimental data is lacking. In the first regard it seems only reasonable to distinguish between diffuse and spoked arcs; between those which project far downstream and those which remain inside the electrode gap; between external fields which dominate and those which are subordinate to the arc self-field; and between predominantly electrothermal and electromagnetic accelerators; not to mention the myriad of gas types and pressures, electrode configurations, and external field orientations and divergences that might influence the conclusions. The problem is compounded by its nonlinearity; that is, the external field may predispose the arc to particular modes in particular regimes, or worse, to instability between two modes. The arc mode selected will in turn determine the effectiveness of the external field in the various functions, and so on. The first task of any analysis is thus to reduce this matrix of conditions to a viable minimum that still retain the essence of the problem.

3.1.2 Arc Modes and Stability

Systematic study of the physics of high current arcs has always been plagued by their inherent instability and hypersensitivity to many environmental factors. From the first studies of simple carbon arcs, through to contemporary work with sophisticated plasma generators, experimental results usually must be qualified by remarks about high and low voltage modes, stable and unstable configurations, localized and diffuse columns, etc., the choice of which seem controlled by obscure, or seemingly trivial factors. The present literature on MPD accelerators reflects this same ambiguity. The existence of high and low voltage modes, and of short and long plumes for the same nominal electrode configuration seems generally accepted, but little systematic criteria have been proposed. Perhaps more crucial is the distinction between diffuse modes which cover the interelectrode annulus more or less uniformly, and spoked modes where arc current is localized in azimuth in a much more intense column. Clearly the former seems preferable for propulsion purposes, both because electrode erosion at given arc power should be much lower and more uniform, and because the propellant stream will be more effectively heated and accelerated if all of it is forced to pass through some portion of the discharge. Despite the elementary importance of this distinction, much of the MPD literature ignores it, or is unconvincing in its assessment. A few references claim to be able to discern diffuse and spoked modes, but the details of

the diagnostics are often sketchy. In one exceptional case, a rotational instability has been clearly identified in a linear Hall accelerator, certain correlations of its onset with field strength and chamber pressure established, and analytical comparison with the Simon-Hoh instability model attempted.[7] In another precise experiment, a pulsed MPD discharge has clearly been shown to pass the bulk of its current in a fin-like radial spoke, rotating at a frequency determined by current and magnetic field strength.[8] Similar behavior has been observed in a steady MPD arc equipped with a segmented electrode.[9] In contrast, other investigators find uniform azimuthal current distribution in their particular steady arcs,[6,10] and pulsed arcs of extremely high currents with no bias field seem to display no tendency to spoking.[11]

In view of the importance of this determination of arc uniformity, it seems curious that suitable indicators are not routinely included in the instrumentation of most arc jet devices, particularly since these could be simply provided. For example, visual confirmation of a rotating spoke could be obtained by observing the arc through a stroboscopic selector, such as a rotating toothed wheel or electronic shutter, or by a high frequency photocell detector. Alternatively, a standard magnetic pickup coil could be inserted through the interelectrode insulator, or even imbedded within it, in such a position to sense any changes in magnetic flux near the plane of the arc, without being exposed to the intense arc environment (see Figure 18). If rotating spokes were present, the probe would record a pulse derivative each time a spoke passed its azimuthal position. Discrimination against total arc current oscillations could be provided by comparison of the response of two such probes at different azimuths, or at different axial positions.
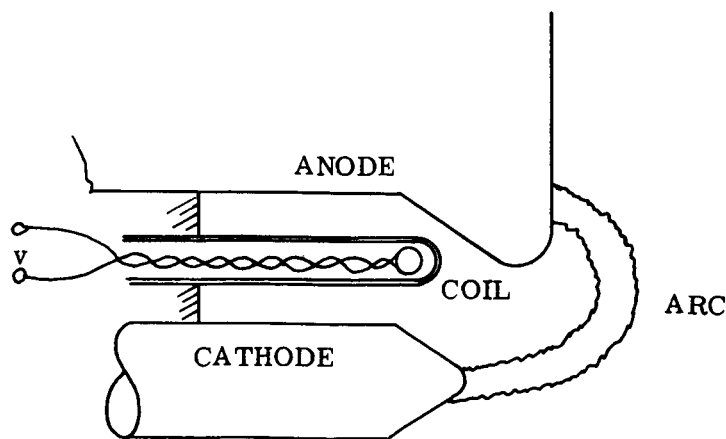

Figure 18. Magnetic Probe for Sensing Arc Spoke Rotation (Schematic)

Likewise perplexing is the dirth of applicable analytical study of the evidently basic stability problem, i.e., the stability of a radial sheet of current between coaxial conductors against collapse to a spoke, with and without external $\overset{\rightharpoonup}{B}$ field. Doubtless such analysis will be mathematically difficult and beset with the usual ambiguities of most plasma stability problems, but any indications it could provide of stable domains of diffuse operation would have direct implication for arc jet performance.

The analogy of this situation to that of conventional chemical rocket motors seems valid and instructive. There too, depending on chamber geometry, pressure, and fuel-oxidizer ratio and types, the motor is capable of controlled, steady combustion with corresponding high performance, or of various modes of unstable operation with exhaust screetch, excessive heat transfer, and otherwise poor performance. Only after the domains of naturally stable operation have been mapped, or instabilities have been inhibited by suitable geometrical changes, is extensive collection or correlation of performance data undertaken. Similar restraint would be beneficial in the further development of the MPD arc. At the least, each submitted data point could be routinely supplemented by description of the arc mode that yielded it.

3.1.3   Self-Field Versus External Field Accelerators

It is commonly assumed that the function and relative importance of the external magnetic field are categorically different for those arc jets which operate at very high currents and thus develop self fields capable of providing the bulk of the $\overset{\rightharpoonup}{j} \times \overset{\rightharpoonup}{B}$ acceleration, and those of lower current which require the external field in order to develop significant electromagnetic body forces. In the former, an external field serves only to "trim" the arc, i.e., to stabilize its pattern in a desired configuration and to channel its exhaust plume. In the latter, the external field is presumed to provide the primary interaction with the arc current, yielding the major component of gas acceleration within the discharge. Thus, while one might conceivably eliminate the external field or reduce it to trivial levels by various alternatives in the high current arcs, its replacement in the second class of MPD accelerator is impossible, by this definition. Unfortunately, much of the experimental data do not completely support this rigid conceptual distinction, nor do they verify this description of the low current accelerator operation.

Historically, the low current MPD arc has at least three ancestors: 1) the electrothermal arc jet -- a conceptually simple, low performance accelerator suffering primarily from conventional heat transfer and frozen flow limitations; 2) the coaxial Hall current accelerator -- a phenomelogically more complicated device of theoretically high, and experimentally low performance; and 3) the high current MPD arc. As mentioned earlier, the low current MPD arc owes its existence to the desire to exploit the MPD high impulse and high efficiency capability at much lower power levels than the self-field device demands. Given

typical arc voltages between 50 and 100 volts, and a power limitation of a few tens of kilo-watts, the available arc currents clearly cannot develop significant self-body forces. To provide electromagnetic forces at this current level, an external field is added, in the familiar $B_{z,r}$ diverging configuration, and interesting performance is thereby indeed obtained. This arrangement may then be regarded as a relative of the coaxial Hall accelerator, a genealogy supported by the common observation that the thrust scales roughly as the product of arc current and applied field, and by the observation of azimuthal Hall current components in a few (but by no means all) MPD devices.

Beyond this point, however, assignment of the low current MPD arc to the Hall family becomes somewhat strained. First, it can be shown theoretically that in a region of full ionization and pressure uniformity where particle acceleration can be neglected, that if the Hall parameter is much larger than unity then no net Hall current flows.[12] Second, a few definitive experiments specifically deny any Hall component of arc current.[8,13] Third, most efficiency versus specific impulse data tend to cluster near the frozen flow curve, suggesting strong electrothermal contribution to the acceleration process. Finally, for given input power, the overall efficiency of this type of accelerator is observed to be rather insensitive to the magnitude of the applied field, over a wide range above a certain small value. Rather, the evident correlation is an increase in arc voltage, and a corresponding decrease in arc current with external field, i.e., an increase in effective arc impedance. While one might attempt to explain this voltage or impedance increase in terms of a higher back emf indicative of more effective gas acceleration, the explicit insensitivity of thermal efficiency to the magnitude of B does not support this interpretation. Instead, the efficiency correlates more closely with power per unit mass flow, i.e., with specific impulse irrespective of the particular values of current and field, again suggesting a basically electrothermal mechanism as an equally viable interpretation. As we discuss below, such electrothermal mechanisms can themselves be quite ambiguous in an environment such as this, and for this and the other reasons mentioned, extraction of the explicit effects of the applied field, and judgment of their intrinsic benefits or detriments can be most obscure.

3.1.4 Electromagnetic Versus Electrothermal Acceleration

It has been pointed out in a previous study[12] that the classical distinction between electromagnetic and electrothermal acceleration mechanisms can become diffuse almost to the point of artificiality when large magnetic fields and tensor conductivities are involved. While the familiar, but clumsy, crossed field or "Faraday" accelerator, with its scalar conduction and low gas temperature is clearly a predominantly electromagnetic device, and the low power arc jet with negligible external field is clearly an electrothermal accelerator, MPD arcs, either of the high or low current variety, are not so readily branded. To be sure, essentially electromagnetic thrust components, such as the streamwise "blowing" provided by $j_r \times B_\theta$ in self-field devices, and essentially electrothermal components derived from

37

scalar joule heating of the plasma can be identified, but these operate in environments conditioned by both magnetic and thermal influences, and are supplemented by a spectrum of hybrid interactions of energetic plasma with the magnetic field pattern which strain the simple definitions. For example, external fields modify the chamber pressure pattern, and thus affect the resistive heating provided by a given arc current. The same fields provide a magnetic "nozzle," where this thermal energy may be in part recovered as streaming energy, or where rotational kinetic energy imparted electromagnetically in the arc may be redirected axially. Axial protrusion of the arc pattern caused by the field may relieve electrode heat transfer somewhat and permit higher arc temperatures, and so on.

The original distinction between electrothermal and electromagnetic accelerators was probably serviceable in the sense that simple electrothermal devices had rather clear limitations on attainable specific impulse and efficiency imposed by material heat transfer and propellant frozen flow considerations, while simple electromagnetic accelerators had totally different, and substantially higher limits determined by the magnitudes of the applied fields which could be tolerated, and by the conductivities of the propellant which could be achieved. In devices as sophisticated as the MPD arcs, little service is left in either the definitions or their related implications. Rather, the more significant questions are which properties of the MPD arc are dominated by the external field, which are beneficial, which are not, and which may be accomplished by other means.

3.1.5   The Body Force Hierarchy

Discussion of the role of the external magnetic field in the MPD accelerator may be facilitated by a brief review of the electromagnetic body force patterns that are predicted by simple magnetogasdynamic theory. In deference to the arc mode uncertainty discussed in Section 3.1.2, we shall consider two idealized models of the arc current pattern, suggested by the available experimental observations as reasonable approximate representations. With reference to Figure 19, we identify a cathode jet (c), an anode jet (a), and a cross conduction zone (b). For simplicity, the cathode and anode jet are assumed purely axial, and the cross-current purely radial. The external field has both axial and radial components and is divergent downstream. The first model, which will represent the diffuse mode, is obtained by revolution of the figure about the indicated centerline through the cathode jet, i.e., the anode jet is in the form of a cylindrical shell, and the cross-current is a circular disc. In the second model, representative of the spoked mode, the anode jet and cross-current will be regarded as tight cylindrical arc column segments like the cathode jet, localized at a specific angular position. Distinction between arcs of large axial protrusion, and those confined close to the electrode gap, is provided by considering different ratios of the anode and cathode jet lengths to the cross-current dimension.
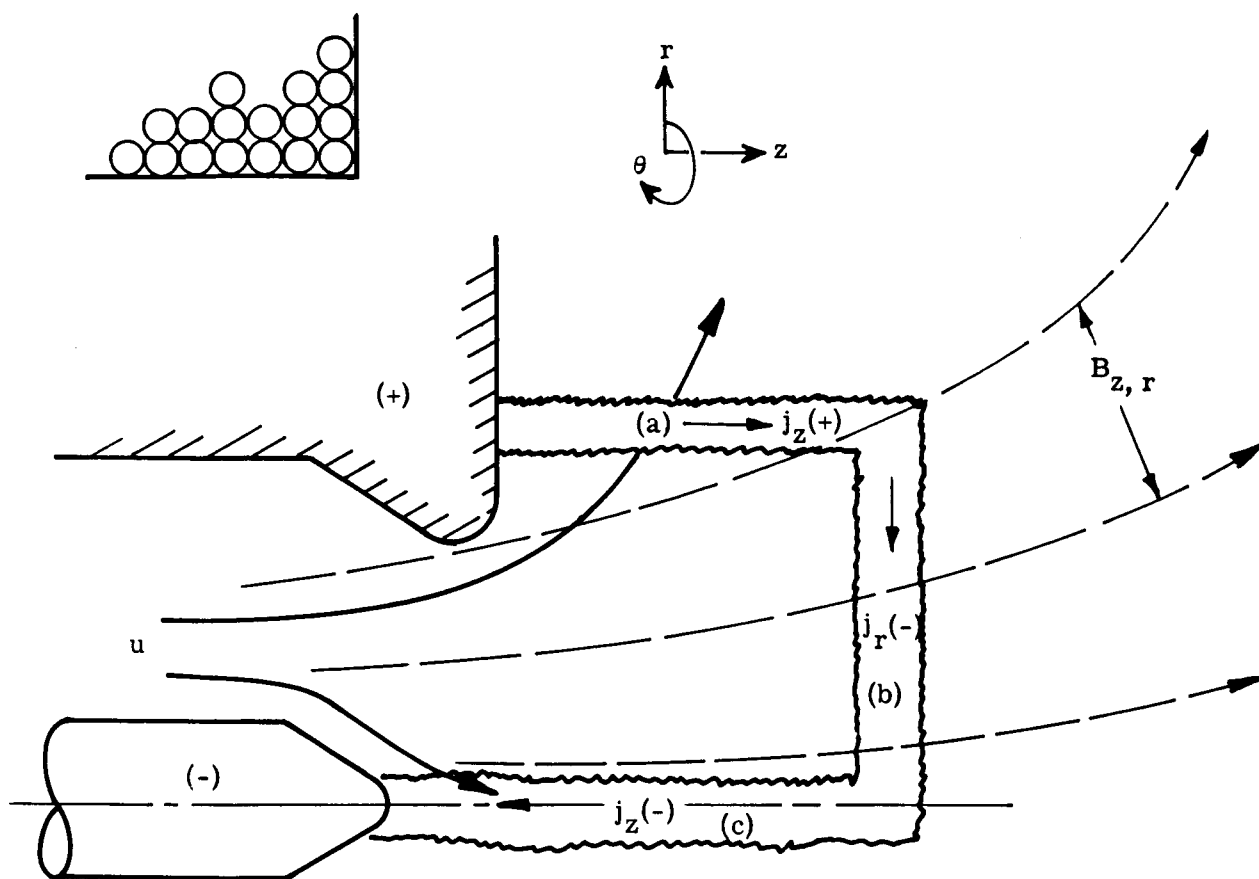
Figure 19.   Idealized Arc and Field Configuration for Body Force Calculations

The necessity of including azimuthal current, j_θ, is a troublesome point which is little clarified by the available experiments.   First, it must be recognized that there are at least three sources of such current: a) true Hall currents which arise from spiraling motion of electrons along $\vec{B}$ lines in relatively low density regions; b) scalar conduction current driven by local electric fields, E_θ; and c) scalar current driven by motional emf, $(\vec{u} \times \vec{B})_\theta$. Theoretical estimates of the magnitudes of these contributions are vague at best, depending as they do on specific local values of the plasma properties which are poorly known.   To retain some generality, we will include j_θ by assumption in certain cases, to illustrate its discernible consequences.

Consider first the diffuse arc model.   In the coordinate system indicated, the applied field components B_z and B_r are positive over the entire arc pattern.   The self-induced field B_θ is everywhere negative and confined to the left of the arc pattern.   Arc current density is positive in (a), negative in (b) and (c).   The direction of the azimuthal currents, j_θ,

cannot be assigned in general, except in those cases where the dominant contribution is identifiable, or where all contributions happen to have the same direction. Presuming j_θ positive for the moment, the force density components, derived from $\vec{f} = \vec{j} \times \vec{B}$, will thus have the following values in the three sections of the arc:

	(a)	(b)	(c)
f_r	$+ j_\theta B_z + j_z B_\theta$	$+ j_\theta B_z$	$+ j_\theta B_z - j_z B_\theta$
f_θ	$+ j_z B_r$	$+ j_r B_z$	-------
f_z	$- j_\theta B_r$	$+ j_r B_\theta - j_\theta B_r$	-------

As a first example, consider a high current arc, with no external field and no azimuthal current density, j_θ, i.e., a pure self-field accelerator. The prevailing body force terms are shown as unbracketed entries in the table below. Note the familiar axial sweeping term acting throughout the cross-current zone, the radial pinching of the cathode jet, and the outward force on the anode jet:

$$\text{Case 1:} \quad B_\theta >> B_{r,z}; \quad j_\theta = 0$$

	(a)	(b)	(c)
f_r	$+ j_z B_\theta$	-------	$- j_z B_\theta$
f_θ	------- $\left[+ j_z B_r\right]$	------- $\left[+ j_r B_z\right]$	-------
f_z	-------	$+ j_r B_\theta$	-------

In brackets are added the first order effects produced by addition of a small external field, B_r, B_z. These act only to swirl the arc, or the gas passing through it, but add no direct increment to the axial thrust or radial containment.

As an opposite extreme, consider next the case of large applied field and low arc current, with again no j_θ admitted. Here we find a primary force pattern which is purely azimuthal. Only when the incremental effect of the small self field is added (bracketed terms) does a direct streamwise force appear:

40

Case 2: $B_{r,z} \gg B_\theta$; $j_\theta = 0$

	(a)	(b)	(c)
f_r	------- $\left[+ j_z B_\theta\right]$	-------	------- $\left[- j_z B_\theta\right]$
f_θ	$+ j_z B_r$	$+ j_r B_z$	-------
f_z	-------	------- $\left[+ j_r B_\theta\right]$	-------

It may be proposed that the rotational kinetic energy imparted to the gas by the azimuthal body forces can be converted into axial streaming by expansion down the "magnetic nozzle" provided by the diverging field, but within the assumptions and approximations employed so far, no force to accomplish this conversion exists. This nozzle effect can be achieved only by admitting azimuthal currents.

To pursue this point further, consider a third case, identical to the second, except that j_θ is now allowed. Here several new force density components appear:

Case 3: $B_{r,z} \gg B_\theta$; $j_\theta \neq 0$

	(a)	(b)	(c)
f_r	$+ j_\theta B_z \left[+ j_z B_\theta\right]$	$+ j_\theta B_z$	$+ j_\theta B_z \left[- j_z B_\theta\right]$
f_θ	$+ j_r B_z$	$+ j_r B_z$	-------
f_z	$- j_\theta B_r$	$- j_\theta B_r \left[+ j_r B_\theta\right]$	-------

Interpretation of this table rests on assignment of the sense and relative magnitude of the azimuthal currents, j_θ. The Hall current contribution will always be in the direction opposite to local $\vec{E} \times \vec{B}$, i.e., negative in this model, and will be largest where $\vec{B}$ is greatest and density lowest. The component driven by E_θ will of course be in the E_θ direction, and will scale with the local scalar conductivity. However, since $\int_0^{2\pi} E_\theta \, d\theta = 0$ around any circle centered on the cathode is required by the geometry, we shall presume $E_\theta = 0$ everywhere in the diffuse model, and neglect this contribution. Finally, the motional component of j_θ has the direction of local $\vec{u} \times \vec{B}$, and a magnitude proportional to this product and to

41

the scalar conductivity. Thus this cannot be evaluated until the flow field is specified, but this is qualitatively evident in the regions of interest. Let us then examine the five j_θ terms in the table, for possible indirect conclusions.

The terms $+ j_\theta B_z$ and $- j_\theta B_r$ in the anode jet represent the magnetic nozzle effect suggested earlier. Fortunately the sense of $- \vec{E} \times \vec{B}$ and $\vec{u} \times \vec{B}$ are the same here and no ambiguity in the direction of j_θ exists. That is, whether the plasma containment is regarded on a free particle basis with electrons trapped into $\vec{E} \times \vec{B}$ drift and ions restrained by a charge separation E field, or on the basis of a continuum conductor streaming across the magnetic field, the induced current is in the $- \theta$ direction, and the body force components are axially outward and radially inward.

The same terms in the cross-current zone (b) can have a similar interpretation, but it is likely that the flow field closely parallels $\vec{B}$ here, and hence the motional j_θ may be unimportant. The $j_\theta B_r$ term, with j_θ a Hall current, is of course the essence of the elementary Hall current accelerator concept, but in view of the definition of (b) as a cross-field conduction zone, this also may be a relatively unimportant element in the composite acceleration process. That is, since $j_r > j_\theta$ here, the small self-field force may still dominate the Hall force in this region.

Finally, there is the $j_\theta B_z$ radial force on the cathode jet. It seems reasonable that this jet entrains incoming gas, at least near the cathode tip, i. e., that u_r is inward and hence $\vec{u} \times \vec{B}$ positive in θ. This is opposite to the sense of the local Hall current, and hence the two effects counteract. A clue to their relative importance is provided by measurements of cathode tip pressure[5, 6] which show an unequivocal decrease in pressure on the axis with increasing applied B. The inference is thus that the motional j_θ dominates the Hall current, and hence the self-constriction of the cathode jet is actually relaxed by the external field. To the extent that the integrated cathode tip pressure contributes to total thrust it thus appears that a strong external field is detrimental to accelerator performance in this particular respect.

Summarizing the diffuse arc model then, it appears that self-magnetic fields are inherently more effective in providing axial acceleration of the gas than are external fields; indeed, unless azimuthal currents are admitted, no first order mechanism for imparting axial body forces can be derived from the applied field. In a sense, then, the appearance of significant azimuthal currents may be taken as an indication of effective external field acceleration; their absence casts doubt on the validity of this process. A premium is thus placed upon their experimental determination.

Turning now to the spoke model of the arc, two significant changes in the above arguments must be made. First, closed azimuthal currents can no longer be allowed in the anode jet (a) and cross-current zone (b); and second, the self-field pattern of the arc is badly distorted

from the simple, cylindrical B_θ field characteristic of the diffuse arc model. Rather, as shown in Figure 20, the self field now encircles the entire arc column, pinching it much
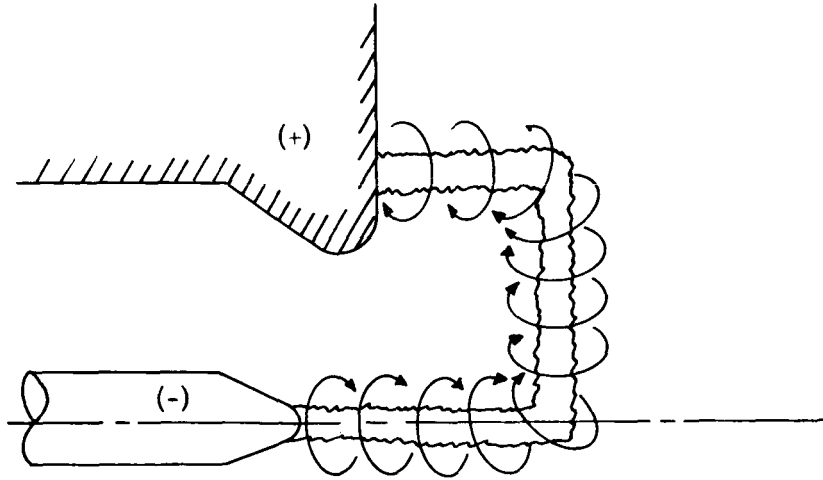

Figure 20. Self Magnetic Field of Spoked Arc (Schematic)

like the cathode jet of the previous model, but exerting a net force which scales as the difference in field strength between one edge of the column and the opposite. This net force is largest near the "corners" of the arc pattern, and dwindles to zero near the center of long segments. In a more realistic arc pattern, curved over its entire length, the net force would scale inversely with the local radius of curvature. Superficially it seems that such a spoked arc would be a less effective self-field electromagnetic accelerator, since it intercepts only a small portion of the incoming flow, but rigorous demonstration of this rests on the details of the interaction of an arc column with a transverse gas flow, -- a topic of considerable complexity and current research interest.

In the case of low arc current and large external field, the spoke model differs from the diffuse mode in lacking all j_θ - derived forces in the anode jet and cross-current column. This leaves only the cathode jet "unpinching" force, which appears to be detrimental to thrust, and the swirling forces, $j_z B_r$ which do not directly impart axial momentum to the gas. The net effect would thus seem to be a rotation of the arc at a speed determined by the arc current and applied field. While this rotation should be advantageous in reducing anode erosion by keeping the attachment point in motion, dynamically it serves only to impart rotational kinetic energy to that portion of the gas flow which is overrun by the rotating spoke.

The effectiveness of the rotating arc in achieving even this azimuthal acceleration of the gas depends on its frequency of rotation, f, on its effective column diameter, d, and on the axial speed of the incoming gas flow, u_z. Crudely speaking, unless $f d \geq u_z$, some of the

gas may be expected to leak through the electrode gap in the azimuthal position away from the arc. If the inequality is satisfied, however, the arc may effectively slice off the incoming flow column, much like the blades of an axial flow compressor. Note that the condition is just satisfied for the conditions $f = 100$ KC; $d = 1$ cm; $u_z = 10^3$ m/sec. If the arc column is thinner, rotates more slowly, or the inlet flow is faster, leakage may be expected. On this basis, strong external fields seem desirable for this mode of operation.

Even presuming that the rotating arc effectively interacts with most of the incoming gas flow, there remains the problem of converting the azimuthal gas momentum, and its associated centrifugal radial motion, into useful axial streaming, in the absence of j_θ currents in the arc. The only recourse here would seem to be to distinguish between the arc column itself, which by geometry cannot embody a closed j_θ, and a more diffuse zone of gas flow heated by previous involvement with the arc which may sustain a diffuse azimuthal current. That is, while the gas which emerges from the arc region has no greater axial momentum than when it entered, it may now be sufficiently conducting that its large centrifugal velocity may profitably interact with the bias field pattern much like the diffuse arc case discussed earlier. If this mechanism functions to nozzle the flow, one should again find an azimuthal current pattern in the exhaust plume downstream of the arc. Presumably the conductivity of this outflow region is considerably lower than that of the arc itself, whether spoked or diffuse. Thus, a stronger magnetic field will be required to accomplish the same degree of plume focusing, and the desirability of large bias fields for effective operation of the spoked mode again seems indicated.

Summarizing the spoke model, then, the high-current self-field process seems inherently less attractive than the diffuse anode, both from an anode erosion standpoint, and from the effectiveness of the axial acceleration process. External field devices will rotate the arc spoke, but appear to exert their primary body forces only in the azimuthal direction, and must rely on magnetic nozzling of the hot gas outflow to derive their axial thrust. The necessity of heating this gas to adequate electrical conductivity adds an electrothermal flavor to the process, even though the rotational kinetic energy and flow re-direction are electromagnetically imparted. Once again, the model clearly demands azimuthal currents in the plume, which should be experimentally measurable.

3.1.6 Critical Velocity and Dynamical Efficiency

Physically and mathematically, the general problem of the MPD accelerator is posed by specifying a geometry; a gas type, flow rate, and chamber pressure or density; an electrode voltage, or total arc current, or total power input; and an external magnetic field configuration. Then, self-consistent operation of a network of physical processes -- epitomized by the fluid conservation equations; equations of state, caloric profile, conductivity function, and other transport coefficients, including all nonequilibrium and rate effects; and

Maxwell's equations including the necessary constituitive relations such as Ohm's law -- determine a solution to the problem. This solution manifests itself physically in two ways: first as a gas outflow of particular velocity, temperature, ionization level, etc., which is usually the focus of our attention, and, in addition, as a current-voltage characteristic of the arc, which can also be instructive. In a sense, the entire device might be regarded as a peculiar electronic tetrode, with an anode and cathode whose voltage-current character-istic can be modulated by a magnetic "grid," and by a gasdynamic "grid." Most of the contributions to the arc voltage are known in a general sense -- a cathode fall to sustain thermionic emission, a column field to sustain adequate arc conductivity, an anode fall to complete current continuity near the cold surface, and a back emf derived from the flux of accelerated conducting gas through the magnetic field, internal or external -- but rigorous calculation of these contributions is not likely to be achieved. Nevertheless, empirical observation of MPD voltage-current characteristics can provide some insight into the in-terior processes of the arc.

One example of this type of information is the correlation of observed arc voltage with a so-called "critical velocity." Specifically, several observers have found that MPD arc voltage roughly fits the form $V = V_0 + u_c Bs$, independent of arc current and mass flow over a broad range, where V_0 is a constant approximately equal to the sum of the elec-trode drops, B is the applied field, s is a characteristic arc dimension, such as the in-terelectrode spacing for short arcs or the total arc length for protruding arcs, and u_c is the "critical velocity," numerically equal to the speed of a propellant molecule when its kinetic energy equals the sum of its dissociation and ionization energies.[14]

Many theories, of varying levels of sophistication, have been proposed to explain this cor-relation, all of which embody, albeit in various subtle forms, the concept of energy equi-partition. This inherent connection between critical velocity and equipartition may be crucial to external field accelerators, in the sense of imposing a limiting dynamical effi-ciency on their conversion of electrical energy to jet kinetic energy. We shall illustrate this point by the simplest possible derivation of the critical velocity. Consider a one-dimensional external field accelerator with orthogonal, uniform electric and magnetic fields and scalar conductivity (Figure 21). Assume that a monatomic gas flow enters the
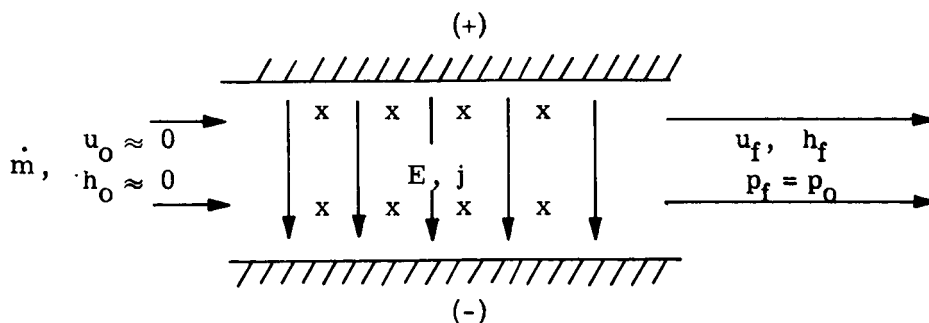

Figure 21. Model of One-Dimensional External Field Accelerator

accelerator with negligible velocity and enthalpy, and leaves with high velocity u_f and enthalpy h_f, but with insignificant pressure change. The momentum and energy equations may then be written in integral form:

$$\int_0^L j\,B\,dx = J\,B \approx \dot{m}\,u_f \tag{1}$$

$$\int_0^L j\,E\,dx = J\,E \approx \dot{m}\,(h_f + u_f^2/2) \tag{2}$$

where $\dot{m}$ is the unit mass flow, and $J = \int_0^L j\,dx$ is the total arc current, irrespective of its distribution. Even if the conductivity of the gas in the discharge is very high, the exhaust velocity has the limiting value imposed by Ohm's law

$$u_f \leq \frac{E}{B} \,. \tag{3}$$

Dividing (2) by (1) and comparing with the equality of (3) yields u_f in the form

$$\frac{1}{2}\,u_f^2 \approx h_f \tag{4}$$

which clearly implies that about 50 percent of the input power is inherently dissipated in heating the gas.

The enthalpy function strictly contains components of random thermal energy ($\frac{5}{2} k\,T$ for each particle, atom, ion, or electron), of electronic excitation of atoms and ions, and of the accumulated ionization energy. If we assume that the gas has been fully ionized (singly), however, the latter component will dominate the others over a broad range of temperature, and we may add the approximation

$$h_f \approx \frac{1}{M}\,\epsilon_i \,, \tag{5}$$

where ϵ_i is the ionization potential of the atom, and the reciprocal of its mass, M, is just the number of atoms per unit mass.

Thus the exhaust velocity is now limited by the ionization potential alone, in the form

$$u_f \approx (2 \, \epsilon_i / M)^{1/2} \, . \tag{6}$$

Returning to (4), the electric field is then also set by ϵ_i:

$$E = u_f \, B \approx (2 \, \epsilon_i / M)^{1/2} \, B \tag{7}$$

and we can piece together the total arc voltage from the electrode falls and integration of (7) along the arc length, s :

$$V = V_0 + E s = V_0 + u_f \, B s = V_0 + (2 \, \epsilon_i / M)^{1/2} \, B \tag{8}$$

which is seen to coincide with the empirical form quoted above with u_f identified as the critical velocity, u_c.

The assumptions of the simple argument outlined here can be relaxed to include two-dimensional flows, non-uniform $\vec{E}$ and $\vec{B}$ fields, Hall current interactions, polyatomic gases, partial ionization, etc., with little change in the basic result. The essential elements in the argument are rather that 1) the acceleration is provided by an external magnetic field; 2) the gas velocity cannot exceed E/B; and 3) the internal energy of the gas is dominated by its ionization (and/or dissociation) energy. The first two elements combine to place an inherent limitation on the dynamical efficiency of the accelerator, i.e., on the fraction of input power which must be degraded to a heating of the gas. The third property simply equates this dissipated power to ionization, and thereby relates the ionization energy to the directed energy. If this identification were not valid, the dissipated energy would merely appear internally elsewhere, e.g., in excitation or other internal modes, or as kinetic temperature. The summary point is thus that the display of a critical velocity by an external field accelerator is essentially an expression of its basic thermodynamic limitations. Note that these limitations transcend the atomic properties of the gas; rather, they are fundamental to this class of electromagnetic acceleration, i.e., to the external $\vec{B}$ field. Only if electrothermal recovery processes are allowed does the particular mode of internal energy storage become a factor in accelerator performance. In this case, the familiar frozen flow criteria resume their applicability. The rough adherence of performance data to frozen flow limits are suggestive in this regard.[15]

The source of the dynamical inefficiency reflected above may be regarded as the inherent mismatch between the imposed electric field, E, and the motional emf, $u B$, along some portion of the channel, in this case near the entrance. In this region, the net effective

47

electric field, $E - uB$, must be supported by large joule currents which heat the gas. Contouring of the applied field profile can modify the situation somewhat, but the essential slip mismatch remains. It is noteworthy, however, that the mismatch is intrinsically less serious for self-field accelerators. To illustrate this point, consider a one-dimensional accelerator with no external field which otherwise conforms to the same conditions applied in the external case. Here the magnetic field is tied to the current density through Maxwell's relation, $\frac{dB}{dx} = -\mu j$, and hence, for uniform j, falls linearly from the value $B_0 = \mu J$ at the channel inlet, to zero at the exit. The momentum equation thus differs from (1) by a factor of $1/2$:

$$\int_0^L j\, B\, dx = \frac{1}{2} J B_0 = \frac{1}{2} \mu J^2 \approx \dot{m}\, u_f \, . \tag{9}$$

The energy equation retains the same form as (2)

$$\int_0^L j\, E\, dx = J E \approx \dot{m}\, (h_f + u_f^2/2). \tag{10}$$

The constraint that u not exceed E/B is still valid, but now must be applied locally since B is not constant, and in particular is zero at the exit. For example, one may find the maximum value of the product uB along the acceleration path, and identify this with the applied electric field. Retaining the assumptions of negligible pressure gradients and uniform current density, relation (9) is valid at any point along the channel and yields the velocity profile

$$u(x) = \frac{j}{\dot{m}} \int_0^x B\, dx = \frac{J}{L\dot{m}} \int_0^x B_0 \left(1 - \frac{x}{L}\right) dx = \frac{\mu J^2}{\dot{m}} \left[\left(\frac{x}{L}\right) - \frac{1}{2}\left(\frac{x}{L}\right)^2\right]. \tag{11}$$

The profile of back emf is thus cubic in $\frac{x}{L}$:

$$u\, B(x) = \frac{\mu^2 J^3}{\dot{m}} \left[\left(\frac{x}{L}\right) - \frac{3}{2}\left(\frac{x}{L}\right)^2 + \frac{1}{2}\left(\frac{x}{L}\right)^3\right] \tag{12}$$

and has a maximum value at $\frac{x}{L} = 1 - \frac{1}{\sqrt{3}}$:

$$\widehat{uB} = \frac{1}{3\sqrt{3}} \frac{\mu^2 J^3}{\dot{m}} \leq E \; . \tag{13}$$

Use of the equality of (13) in (10), followed by comparison with (9) yields the self field partition ratio

$$\frac{h_f}{\frac{1}{2} u_f^2} = \frac{8\sqrt{3}}{9} - 1 = 0.54 \tag{14}$$

compared to unity for the external field case. Note also that the E/B limit on u_f has also been relaxed. Here

$$u_f = 2.6 \frac{E}{B_0} \; . \tag{15}$$

Despite the crudeness of the above arguments, the essential physical point involved here is that the self-magnetic field inherently decreases along the acceleration path, and hence it is possible to match the back emf product uB more closely to a constant applied electric field. The joule dissipation is thereby reduced and the acceleration is dynamically more efficient.

3.1.7 Summary

The admittedly sketchy and disconnected thoughts presented above by no means resolve any of the ambiguities of the MPD arc, nor provide a definitive answer to the question implicit in the title. Rather they are advanced in the spirit of encouraging more detailed study of certain aspects of the external magnetic field interactions before categorically accepting the logistical complications and propulsion system disadvantages of these techniques. Particularly, the following points have been raised:

1. MPD arcs give evidence of ability to operate in a variety of substantially different geometrical configurations. It seems almost imperative to ascertain the prevailing mode before attempting to examine the effects introduced by external magnetic fields, or any other physical aspect of the accelerator, or before attempting to correlate performance data. Thorough experimental and theoretical survey of the arc mode domains could provide a basis for controlled selection of optimum modes for given ranges of operation.

2. If it is unavoidable that the arc run in a spoked mode, an external field is clearly beneficial in moving the anode attachment point rapidly enough to prevent anode surface damage. If all of the incoming flow is to be intimately involved with the arc, the arc should rotate at least at the frequency $u_z d$,

where u_z is the inlet flow velocity and d the effective arc breadth in the streamwise direction, z.

3. Many empirical observations combine to cast doubt on the effectiveness of an external field in providing streamwise electromagnetic acceleration. Rudimentary analyses of the body force distributions likewise indicate that the external field acceleration process is sufficiently indirect that it may be impaired by second-order effects, or small scale disturbances, as yet unidentified. Particularly troublesome is the necessity for large azimuthal currents in the streamwise acceleration and radial containment processes. Whether these are Hall currents or motionally induced scalar currents depends on the local conditions, but neither type have as yet been experimentally identified with convincing regularity.

   In contrast, self-field accelerators seem experimentally and analytically more tractable, provided the requisite power densities can be provided.

4. The appearance of "critical velocity" or "critical potential" tendencies in an MPD arc may be indicative of dissipative energy equipartition characteristic of acceleration in uniform electric and magnetic fields. Since the gas in an external field device must go through at least two stages of such acceleration, once to acquire azimuthal momentum in the arc zone, and again to convert to axial motion in the magnetic nozzle, these dynamical losses may compound to serious proportions.

   Again, by contrast, self-field acceleration is inherently more efficient dynamically because of its intrinsic self-field contour, and it requires only one, streamwise, acceleration event.

As a parallel program to the study of the above points, it would be worthwhile to evaluate alternative methods of achieving the beneficial functions of an external B field. That is, if one should become convinced that the concept of external field acceleration is basically unproductive in this environment, and that only electrothermal and self-field electromagnetic processes can function effectively, then the peripheral benefits of the bias field might be provided equally well by other means, e.g., the plume might be channeled gasdynamically, or the arc might be swirled or diffused by a more sophisticated anode structure, etc. It is not the topic of this paper to explore these, but it may well turn out that the optimum compromise involves an electrothermal/self-electromagnetic accelerator, trimmed by an external field sufficiently weak that no substantial detriment to arc operation or system weight is incurred, and further aided by such mechanical, electrical or gasdynamic contrivances.

3.2   Hall and Radial Current Variation and Plasma Motion in an MPD Arc, by R. P. Treat

3.2.1   Introduction

Although the experimental picture of the exact distribution of the arc current density and its dependence on the arc parameters is not completely clear, the general shape of the current distribution in the coaxial electrode configuration is known to consist of a central core emanating from the cathode and then forming a return path to the anode in an umbrella-like or rotating fan-like distribution.[8, 9, 16, 17, 18] The current is usually confined to a region extending 20 or 30 centimeters axial distance from the cathode tip. The theory of the current flow is not very well developed and some properties of the arc are not understood satisfactorily. For example, a large radial current flow is sometimes found to develop in the throat of the configuration, which is somewhat surprising in view of the large values of the Hall parameter there.[16, 17] Further, the role of the Hall current in the acceleration of the plasma and in the current flow has not been clarified.[15] In some cases a Hall current has not been detected in regions where radial currents exist and where the Hall parameter is significantly large, where it is expected on the basis of the coupling of radial and Hall currents shown by the current equation for crossed electric and magnetic fields.[8, 16, 17]

In the MPD arc, an unionized element of gas flows into a region where the discharge forms and then flows through the discharge and is finally ejected in a current-free, strongly ionized, electrically neutral, axially directed jet. During and after the ionization, pressure gradients and Lorentz forces accelerate the element until the electric field viewed from a coordinate frame moving with the gas element vanishes. In this investigation we consider the growth and decay of the current density following an arbitrary gas element through the discharge. In the analysis we acknowledge the ionization and acceleration of the gas and its effect on the current density variation. The case where the applied field is strong compared with the fields induced by the arc currents and the magnetic pressure is comparable to or larger than the plasma kinetic pressure is considered.

The generalized current equation which is employed and some of the basic assumptions which enter into the analysis are given in Section 3.2.2, where we also introduce the other basic equations and the notation which are used and proceed with the mathematical formulation of the analytical model. In Section 3.2.3, the simultaneous icnization and acceleration of the gas and the variation of the current density following the motion of a plasma element is considered for the case of weak ionization. Solutions of the equations governing the plasma motion and the variation of the current density are given in Section 3.2.4 for the case of strong ionization. In Section 3.2.5 the extent to which the analysis applies to the actual physical situation is considered.

51

3.2.2   Basic Equations and Fundamental Assumptions

We will consider the temporal change of the current density following the motion of an arbitrary gas element through the discharge region of a standard coaxial electrode configuration of an MPD arc jet. A basic assumption of this analysis is that the Boltzmann equation holds for a plasma consisting of monatomic hydrogen, protons and electrons. The Boltzmann equation for the α th species is

$$\frac{\partial f_\alpha}{\partial t} + v_\alpha^k \frac{\partial f_\alpha}{\partial x^k} + \frac{F_\alpha^k}{m_\alpha} \frac{\partial f_\alpha}{\partial v_\alpha^k} = \left(\frac{\partial f_\alpha}{\partial t}\right)_{coll} , \tag{1}$$

where α stands for h, e or p to indicate hydrogen, electron or proton. Latin indices i, j, k, .. = 1, 2, 3 denote the components of vectors and tensors in a cartesian coordinate system x^k. The convention of summing over repeated upper and lower indices will be followed. In (1), f_α is the Boltzmann distribution function for the α th species, $\left(\frac{\partial f}{\partial t}\right)_{coll}$ is the rate of change of f_α due to collisions, v_α^k is the particle velocity and

$$F_\alpha^k = q_\alpha \left(E^k + \epsilon^{kij} v_i B_j\right) \tag{2}$$

is the electromagnetic force acting on a particle. The cartesian components of the electric and magnetic field vectors are given by E^k and B_j, q_α is the electric charge of the α th species and ϵ^{ijk} is the totally antisymmetric tensor with $\epsilon^{123} = 1$.

The continuity equation is obtained from the Boltzmann equation by multiplying (1) by the mass per particle, integrating over velocity and summing over the species present in the plasma. The result is

$$\frac{\partial \rho}{\partial t} + \frac{\partial \rho v^k}{\partial x^k} = 0 , \tag{3}$$

where v^k is the mass velocity and ρ is the mass density of the plasma. Multiplying the Boltzmann equation by the momentum per particle, using (2) for F_α^k, integrating over velocity and summing over species yields, with the aid of (3), the momentum equation

$$\rho \frac{\partial v^k}{\partial t} + \rho v^j \frac{\partial v^k}{\partial x^j} = - \frac{\partial p^{jk}}{\partial x^j} + \epsilon^{kij} j_i B_j + \omega \left(E^k + \epsilon^{kij} v_i B_j\right) , \tag{4}$$

where ω is the electric charge density and p^{jk} is the kinetic pressure tensor defined by

$$p^{jk} = \sum_{\alpha} p_{\alpha}^{jk} , \qquad (5)$$

and

$$p_{\alpha}^{jk} = \int m_{\alpha} u_{\alpha}^{j} u_{\alpha}^{k} f_{\alpha} \, dv_{\alpha} . \qquad (6)$$

In (6), dv_{α} denotes a three-dimensional infinitessimal element of velocity space and the random particle velocity in the integrand is defined by

$$v_{\alpha}^{k} = v^{k} + u_{\alpha}^{k} . \qquad (7)$$

To obtain an equation of change for the electric current density which is sufficiently general for the problem of interest here we proceed as follows. Multiplying the Boltzmann equation by the current per particle $q_{\alpha} v_{\alpha}^{j}$, inserting the expression for the force as given by (2), integration over velocity and summation over species yields

$$\frac{\partial j^{k}}{\partial t} + \frac{\partial}{\partial x^{j}} \left(- \omega v^{j} v^{k} + j^{j} v^{k} + \frac{e}{m_{p}} p_{p}^{jk} + \frac{e}{m_{e}} p_{e}^{jk} \right) + e^{2} \left(\frac{n_{e}}{m_{e}} + \frac{n_{p}}{m_{p}} \right) E^{k}$$

$$+ e^{2} \left(\frac{n_{e}}{m_{e}} \bar{v}_{ej} + \frac{n_{p}}{m_{p}} \bar{v}_{pj} \right) B_{i} \, \epsilon^{jik} = \sum_{\alpha} q_{\alpha} v_{\alpha}^{k} \left(\frac{\partial f}{\partial t} \right)_{coll} dv_{\alpha} . \qquad (8)$$

where the average particle velocities are determined by

$$\bar{v}_{\alpha}^{j} = \frac{1}{n_{\alpha}} \int v_{\alpha}^{j} f_{\alpha} \, dv_{\alpha} . \qquad (9)$$

We prefer to deal with the mass velocity, electric current density, charge density ω, mass density and ionization fraction ϵ, rather than the electron and proton number densities and average particle velocities $\bar{v}_{e}^{j}$ and $\bar{v}_{p}^{j}$. To express (8) in terms of the desired variables we have the algebraic equations

$$\rho = m_{e} n_{e} + m_{p} n_{p} + m_{h} n_{h} ,$$

$$\omega = - e n_{e} + e n_{p} , \qquad (10)$$

$$\epsilon = \frac{n_{p}}{n_{h} + n_{p}} ,$$

and

$$\rho v^j = m_e n_e \bar{v}_e^j + m_p n_p \bar{v}_p^j + n_h m_h \bar{v}_h^j ,$$

(11)

$$j^j = - e n_e \bar{v}_e^j + e n_p \bar{v}_p^j .$$

We shall assume that the charge exchange and elastic collisions between neutrals and protons are sufficiently frequent so that their relative velocity remains negligible. This provides us with the additional equation

$$\bar{v}_p^j = \bar{v}_h^j .$$

(12)

From (10), (11) and (12) one can determine n_e, n_p, $\bar{v}_p^j$ and $\bar{v}_e^j$ in terms of ρ, ω, ϵ, j^j and v^j. Substituting the resulting expressions in (8) gives, after neglecting m_e/m_p compared with unity,

$$\frac{\partial j^k}{\partial t} + \frac{\partial}{\partial x^j} \left(v^k j^j + v^j j^k - \omega v^j v^k - \frac{e}{m_e} p_e^{jk} \right) =$$

$$\epsilon \beta \left(E^k + \epsilon^{jik} v_j B_i \right) - \frac{\omega e^2}{m_e} E^k - \frac{e}{m_e} \epsilon^{jik} j_j B_i + \sum_\alpha \int q_\alpha v_\alpha^k \left(\frac{\partial f_\alpha}{\partial t} \right)_{coll} dv_\alpha ,$$

(13)

where, for conciseness we have introduced the parameter

$$\beta = \frac{e^2 \rho}{m_e m_p} .$$

(14)

The collision term in (13) is given in terms of the resistivity η by

$$\eta j^k = \frac{1}{\epsilon \beta} \sum_\alpha \int q_\alpha v_\alpha^k \left(\frac{\partial f_\alpha}{\partial t} \right)_{coll} dv_\alpha .$$

(15)

In (13) we have neglected $\frac{m_e}{m_p} p_p^{jk}$ compared with p_e^{jk}. In the following we shall assume scalar pressures and charge neutrality, whereby (4) and (13) simplify to

$$\rho \frac{D\vec{v}}{Dt} = - \text{grad } p + \vec{j} \times \vec{B} ,$$

(16)

54

$$\frac{D\vec{j}}{Dt} = \epsilon \beta (\vec{E} + \vec{v} \times \vec{B}) - \frac{e}{m_e} \vec{j} \times \vec{B} + \frac{e}{m_e} \text{grad } p_e - \nu_c \vec{j} - \vec{j} \cdot \text{grad } \vec{v} - \vec{j} \text{ div } \vec{v} \ , \quad (17)$$

where the collision frequency ν_c is determined by

$$\eta = \frac{m_e \nu_c}{e^2 n_e} \ , \quad (18)$$

and

$$\frac{D}{Dt} = \frac{\partial}{\partial t} + \vec{v} \cdot \text{grad}$$

is the total time derivative with respect to the plasma mass motion. Equation (17) reduces to the so-called generalized Ohm's law[19] for full ionization and neglect of the terms which are quadratic in $\vec{j}$ and $\vec{v}$.

In the following analysis we will consider a situation where the applied magnetic field is much larger than the field induced by arc currents and the magnetic pressure of the applied field is comparable to the plasma kinetic pressure. These conditions are satisfied in low pressure MPD arcs which operate at 10 to 100 mm arc chamber pressure at applied fields of 1000 gauss and more.[5, 6] We shall then consider the plasma acceleration and distribution of the arc current density ignoring entirely the effect of the self induced fields. Moreover, we will neglect the pressure gradients compared with the Lorentz forces, so we will be considering the idealized case of pure electromagnetic acceleration in the arc. The problem is simplified further by considering, instead of the coaxial geometry of the MPD arc, plane parallel electrodes with uniform crossed electric and magnetic fields. For application to the MPD arc this means neglecting Coriolis and centrifugal forces in the momentum equation and analogous terms in the current equation (17) and neglecting nonuniformities of the electric field and axial applied magnetic field that arise in a coaxial geometry.

In the equations of change (16) and (17) for the velocity and the current density we shall neglect the time rate of change at a fixed position compared with the convective rate of change of velocity and current density vectors. However, arcs which are rotating in the manner found by Lovberg[8] and Larson[9] and which are not steady, but where the partial time derivative of plasma variables may be small compared with the local convective rates of change may also lie in the domain of application of the analysis. With this analytical model let us first consider the ionization of a gas element as it passes into a region where the discharge forms.

3.2.3 Ionization and Acceleration of the Flow

Let us assume that in the ionizing region the flow is incompressible. This is probably a good assumption, since while the ionization is proceeding the electrical energy should go mainly into the excitation and ionization of neutral particles rather than accelerating the flow. For a steady incompressible flow we have

$$\frac{\partial v^k}{\partial x^k} = 0 \ . \tag{19}$$

When there is ionization, continuity of electron number density is expressed by

$$\frac{\partial n_e \bar{v}_e^k}{\partial x^k} = \nu_I (x^j) n_e \ , \tag{20}$$

where the ionization frequency is given by

$$\nu_I (x^j) = \langle v_e \sigma_I \rangle n_h = \frac{n_h}{n_e} \int v_e \sigma_I f_e dv_e \ , \tag{21}$$

σ_I is the ionization cross section and v_e is the magnitude of the electron velocity. Because of charge neutrality, charge conservation and the definition of the electric current density we have

$$- \frac{\partial n_e \bar{v}_e^k}{\partial x^k} + \frac{\partial n_e \bar{v}_p^k}{\partial x^k} = 0 \ .$$

This equation together with the no ion-slip condition, the neglect of m_e/m_p compared with unity and use of (19) yields from (20)

$$\frac{dn_e}{dt} = \nu_I (x^j) n_e \ , \tag{22}$$

where

$$\frac{d}{dt} = v^k \frac{\partial}{\partial x^k} \tag{23}$$

denotes the time derivative following a steady motion. Accordingly, the time t is

henceforth to be regarded as a parameter on a stream line of the motion. Now with the definition of ϵ and to accuracy m_e/m_p compared with unity, (22) can be written as

$$\frac{d\epsilon}{dt} = \nu_I \epsilon (1 - \epsilon) , \tag{24}$$

where ν_I without the argument x^j indicates the ionization frequency if the gas were completely unionized, i.e.,

$$\nu_I = \langle v_e \sigma_I \rangle \left(n_p + n_h \right) . \tag{25}$$

In view of the incompressibility, and if possible changes in the Boltzmann electron distribution function is ignored, ν_I is constant on a stream line. Equation (24) may then be integrated along a stream line with the result

$$\epsilon = \left[1 + \left(\frac{1 - \epsilon_0}{\epsilon_0} \right) \exp(- \nu_I t) \right]^{-1} , \tag{26}$$

where ϵ_0 is the ionization fraction at the initial point of a motion of a gas element on a stream line. For

$$\frac{\epsilon_0}{1 - \epsilon_0} \exp(\nu_I t) \ll 1 , \tag{27}$$

the ionization fraction is approximated by

$$\epsilon = \epsilon_0 \exp(\nu_I t) . \tag{28}$$

Returning to (17) we make the simplifying approximations of neglecting the terms in the current equation which are proportional to the electron pressure gradient and the velocity gradient in the direction of the current flow compared with the term $\frac{e}{m_e} \vec{j} \times \vec{B}$, which is consistent with the assumption that the Lorentz force is dominant in the momentum equation. With these approximations and conditions stated on page 55, we have the following simplified momentum and current equations.

$$\rho \frac{d\vec{v}}{dt} = \vec{j} \times \vec{B} , \tag{29}$$

$$\frac{d\vec{j}}{dt} = \epsilon(t) \beta (\vec{E} + \vec{v} \times \vec{B}) - \frac{e}{m_e} \vec{j} \times \vec{B} - \nu_c \vec{j} , \tag{30}$$

where $\epsilon(t)$ is given by (26), or in the case of weak ionization, by (28). In (29) and (30) the induced field is neglected, ρ is constant on a stream line and the electric and magnetic fields E_x and B_z are uniform. In the discussion we will comment on some of the consequences of neglecting the induced magnetic field and the pressure forces in the momentum balance. Writing out the component equations of (29) and (30) and dividing by the collision frequency ν_c yields

$$\frac{dv_x}{d\tau} = \frac{B_z}{\rho \nu_c} j_y \ , \tag{31}$$

$$\frac{dv_y}{d\tau} = - \frac{B_z}{\rho \nu_c} j_x \tag{32}$$

$$\frac{dj_x}{d\tau} = \frac{\epsilon \beta B_z}{\nu_c} v_y' - \Omega j_y - j_x \ , \tag{33}$$

$$\frac{dj_y}{d\tau} = - \frac{\epsilon \beta B_z}{\nu_c} v_x + \Omega j_x - j_y \ , \tag{34}$$

where

$$v_y' = \frac{E_x}{B_z} + v_y \ , \tag{35}$$

the dimensionless time

$$\tau = \nu_c t \ , \tag{36}$$

has been introduced and

$$\Omega = \frac{e B_z}{m_e} \tag{37}$$

is the electron Hall parameter with the sign of B_z retained in the definition. We have omitted the z-component of the momentum and current equations because they are uncoupled to the x and y components by virtue of neglecting the induced magnetic field.

We will now consider the conditions for which the motion of the plasma affects the formation of the current distribution while the ionization is proceeding. Eliminating v_y' and v_x from (33) and (34) with the aid of the integrals of (31) and (32) yields

$$\frac{dj_x}{d\tau} = \frac{\epsilon \beta E_x}{\nu_c} - \frac{m_e}{m_p} \Omega^2 \epsilon(\tau) \int_0^\tau j_x d\tau - \Omega j_y - j_x \, , \tag{38}$$

$$\frac{dj_y}{d\tau} = - \frac{m_e}{m_p} \Omega^2 \epsilon(\tau) \int_0^\tau j_y d\tau + \Omega j_x - j_y \, . \tag{39}$$

The integrals represent the damping effect on the growth of the current which is caused by the motion of the plasma. Let us consider the magnitude of these terms during the ionization of the flow. The integral in (38) is of the order of or less than

$$\epsilon \frac{m_e}{m_p} \Omega^2 \frac{\nu_c}{\nu_I} j_x \, .$$

Comparing this term with the last term in (38) shows that the motion of the plasma will have a negligible effect on the j_x component of the current density if

$$\epsilon \frac{m_e}{m_p} \Omega^2 \frac{\nu_c}{\nu_I} << 1 \, . \tag{40}$$

The same holds for (39), so both the Hall current and the component parallel to the electric field will be unaffected by the plasma motion if (40) is satisfied. Writing the above inequality in the form

$$\frac{\omega_e}{(\nu_c \nu_I)^{1/2}} << \left(\frac{m_p}{\epsilon m_e}\right)^{1/2} \tag{41}$$

we see that in a region of weak ionization, say $\epsilon < 0.01$, the inequality (41) will be satisfied except for large values of the parameter $\omega_e/(\nu_c \nu_I)^{1/2}$ which for the magnitude of the magnetic field and pressure considered here would occur only if the Hall parameter is large in the breakdown region and the ionization frequency is very much less than the elastic collision frequency. In the case of very strong ionization, for example, if $\omega_e/(\nu_I \nu_c)^{1/2}$ is of the order of 10, then the inequality (41) would not be satisfied and motional damping before the ionization is completed would be a possibility.

In the case of weak ionization, when (41) is satisfied we may omit the integrals in (38) and (39) and use (28) for the time dependence of $\epsilon(\tau)$. The equations can then be integrated with the result

$$j_x = \frac{\sigma(o) E_x (1 + \nu_I/\nu_c)}{(1 + \nu_I/\nu_c)^2 + \Omega^2} \exp\left(\frac{\nu_I}{\nu_c} \tau\right) + \exp(-\tau)(A_1 \sin \Omega\tau + A_2 \cos \Omega\tau) , \qquad (42)$$

$$j_y = \frac{\sigma(o) E_x \Omega}{(1 + \nu_I/\nu_c)^2 + \Omega^2} \exp\left(\frac{\nu_I}{\nu_c} \tau\right) + \exp(-\tau)(A_2 \sin \Omega\tau - A_1 \cos \Omega\tau) , \qquad (43)$$

where

$$\sigma(o) = \frac{n_e(o) e^2}{m_e \nu_c}$$

is the initial scalar conductivity and A_1 and A_2 are arbitrary constants. If $\nu_I/\nu_c \ll 1$, then the oscillatory part of the solution damps out much faster than the exponential increase of the current density and after a few collision times we have

$$j_x \approx \frac{\sigma(o) E_x}{1 + \Omega^2} \exp\left(\frac{\nu_I}{\nu_c} \tau\right) , \qquad (44)$$

$$j_y \approx \frac{\sigma(o) E_x \Omega}{1 + \Omega^2} \exp\left(\frac{\nu_I}{\nu_c} \tau\right) , \qquad (45)$$

which are the solutions one obtains when the convective rate of change of the current density is neglected. Hence, if $\nu_I/\nu_c \ll 1$, for times larger than a few collision times we need not consider $d\vec{j}/dt$ in the current equations (33) and (34).

3.2.4   Plasma Acceleration and Current Density Variation for Strong Ionization

For full ionization we have $\epsilon = 1$ in (31) to (34) and we can integrate the system of equations. The general solution consists of a linear combination of exponentials $\exp(\lambda\tau)$. The characteristic roots λ satisfy the equation

$$\left[\lambda(\lambda + 1) + \frac{m_e}{m_p} \Omega^2\right]^2 + \Omega^2 \lambda^2 = 0 . \qquad (46)$$

Hence

$$\lambda^2 + (1 \mp i\Omega)\lambda + \frac{m_e}{m_p} \Omega^2 = 0 . \qquad (47)$$

If λ is a root then $\bar{\lambda}$, the complex conjugate of λ, is also a root. Solving (47) for the negative sign on the complex part of the coefficient of λ gives the two roots

$$\lambda_1 = -\frac{1}{2}(1 - i\Omega) + \frac{1}{2}\left[(1 - i\Omega)^2 - \frac{4\,m_e}{m_p}\,\Omega^2\right]^{1/2} ,$$

$$\lambda_2 = -\frac{1}{2}(1 - i\Omega) - \frac{1}{2}\left[(1 - i\Omega)^2 - \frac{4\,m_e}{m_p}\,\Omega^2\right]^{1/2} .$$

(48)

To accuracy of m_e/m_p compared with unity the roots are given by

$$\lambda_1 = -\varkappa - i\varkappa\Omega ,$$

$$\lambda_2 = -1 - i\Omega ,$$

(49)

where, for conciseness, we have introduced the notation

$$\varkappa = \frac{m_e}{m_p}\left(\frac{\Omega^2}{1 + \Omega^2}\right) .$$

(50)

Since $\Omega^2/(1 + \Omega^2)$ is never greater than unity, $\varkappa$ is smaller than the ratio of the electron to proton masses.

A solution is determined uniquely when the initial conditions are specified. We take as initial values

$$v_x = v_y = 0 ,$$

(51)

$$j_x = j_y/\Omega = \frac{\sigma E_x}{1 + \Omega^2} ,$$

where

$$\sigma = \frac{n_e e^2}{m_e \nu_c} .$$

(52)

These initial conditions assume that a steady current distribution and full ionization is reached before the onset of motional damping. The conditions for which this is possible have been discussed in the preceding section. With initial conditions (51) the solution of (31) to (34) is

61

$$v_x = \frac{E_x}{B_z (1 - \varkappa)} \left(\exp(-\varkappa\tau) \sin \varkappa\Omega\tau - \varkappa \exp(-\tau) \sin \Omega\tau \right) , \tag{53}$$

$$v_y = -\frac{E_x}{B_z (1 - \varkappa)} \left[(1 - \exp(-\varkappa\tau) \cos \varkappa\Omega\tau) - \varkappa (1 - \exp(-\tau) \cos \Omega\tau) \right] , \tag{54}$$

$$j_x = \frac{\sigma E_x}{(1 + \Omega^2)(1 - \varkappa)} \left[\exp(-\varkappa\tau)(\cos \varkappa\Omega\tau + \Omega \sin \varkappa\Omega\tau) \right.$$
$$\left. - \exp(-\tau)(\cos \Omega\tau + \Omega \sin \Omega\tau) \right] , \tag{55}$$

$$j_y = \frac{\sigma E_x}{(1 + \Omega^2)(1 - \varkappa)} \left[\exp(-\varkappa\tau)(- \sin \varkappa\Omega\tau + \Omega \cos \varkappa\Omega\tau) \right.$$
$$\left. - \exp(-\tau)(- \sin \Omega\tau + \Omega \cos \Omega\tau) \right] . \tag{56}$$

The terms in the equations (53) to (56) which are proportional to $\varkappa$ are small compared with the remaining terms. Moreover, they decay faster by a factor m_e/m_p than the other terms. We see that, as in the case of weak ionization, if only times much larger than a collision time are to be considered then we need not include the convective rate of change of the current density. We will not be concerned further here with the small amplitude rapidly decaying terms. The part of the solution of interest here is

$$v_x = \frac{E_x}{B_z} \exp(-\varkappa\tau) \sin \varkappa\Omega\tau , \tag{57}$$

$$v_y = -\frac{E_x}{B_z} \left[1 - \exp(-\varkappa\tau) \cos \varkappa\Omega\tau \right] , \tag{58}$$

$$j_x = \frac{\sigma E_x}{1 + \Omega^2} \exp(-\varkappa\tau)(\cos \varkappa\Omega\tau + \Omega \sin \varkappa\Omega\tau) , \tag{59}$$

$$j_y = \frac{\sigma E_x}{1 + \Omega^2} \exp(-\varkappa\tau)(- \sin \varkappa\Omega\tau + \Omega \cos \varkappa\Omega\tau) , \tag{60}$$

where we have neglected $\varkappa$ compared with unity. The mass velocity and current density show a damped oscillation following the motion of a plasma element. The amplitudes of the Hall component of the current and the components of the current and velocity in the direction

of the electric field decay exponentially with the time constant

$$t_d = 1/\varkappa \nu_c \tag{61}$$

which is, according to the definition of $\varkappa$, three orders of magnitude longer than the Coulomb collision time if Ω is greater than unity, and longer if Ω is less than unity. The plasma velocity perpendicular to E_x and B_z approaches the steady drift velocity $- E_x/B_z$ exponentially with the time constant (61). Together with the v_x and v_y components there is a v_z component of the velocity established by the initial flow of the gas and increased by a negative pressure gradient in the z-direction and by a Lorentz force arising from the self field and the arc currents. Hence, when the solution is applied to a coaxial geometry, it shows a spiraling motion with damped radial and azimuthal oscillations superimposed upon it.

Integration of (57) gives

$$x - x_0 = \frac{E_x \exp{(-\varkappa \tau)}}{\nu_c B_z (1+\Omega^2) \varkappa} (-\sin \varkappa \Omega \tau - \Omega \cos \varkappa \Omega \tau) + \frac{E_x \Omega}{\nu_c B_z (1+\Omega^2) \varkappa} , \tag{62}$$

where x_0 is the x-coordinate of the initial position of the gas element. For $\varkappa \tau \to \infty$ we have

$$x - x_0 \bigg|_{\varkappa \tau \to \infty} = \frac{E_x}{\omega_p B_z} , \tag{63}$$

where ω_p is the proton gyro-frequency including the sign of the magnetic field. Interpreted in a coaxial geometry, (63) shows a net radial displacement toward the axis independent of the positive or negative axial orientation of the magnetic field. For $E_x = -5000$ volts/ meter and $B_z = 0.1$ Webers/meter^2, values which are common in MPD arc operation, we have

$$x - x_0 = 5 \times 10^{-3} \text{ meters },$$

which is comparable to the anode radius at the throat of this device. The maximum radial inward displacement occurs for $\varkappa \Omega \tau = \pi$ and from (62) is seen to be

$$(x - x_0)_{max} = \frac{E_x}{\omega_p B_z} \left[\exp{(-\pi/\Omega)} + 1\right] , \tag{64}$$

which at most is twice the displacement for $\varkappa \tau \to \infty$. The y-displacement is given by

$$y - y_0 = -\frac{E_x \tau}{B_z \nu_c} + \frac{E_x}{\omega_p B_z} \left[1 - \exp{(-\varkappa \tau)}(\cos \varkappa \Omega \tau + \Omega \sin \varkappa \Omega \tau)\right] \tag{65}$$

63

From (65) it is seen that for $\varkappa \tau \gg 1$

$$y - y_o \approx - \frac{E_x}{B_z \omega_p} (\omega_p t - 1) ,$$

and for times long compared with the proton gyro-frequency the y-displacement is the drift velocity multiplied by the time.

As shown in Section 3.2.3, if the ratio of the ionization frequency to the elastic collision frequency is much less than unity we may neglect the convective rate of change of the current density in (33) and (34). Then we obtain, by solving (33) and (34), the current density components

$$j_x = \frac{\epsilon \beta B_z}{\nu_c (1 + \Omega^2)} (\Omega v_x + v'_y) ,$$

$$j_y = \frac{\epsilon \beta B_z}{\nu_c (1 + \Omega^2)} (- v_x + \Omega v'_y) .$$

When these components are substituted in (31) and (32) we obtain

$$\frac{1}{\epsilon \varkappa} \frac{dv_x}{d\tau} = - v_x + \Omega v'_y , \tag{66}$$

$$\frac{1}{\epsilon \varkappa} \frac{dv'_y}{d\tau} = - \Omega v_x - v'_y , \tag{67}$$

where $\varkappa$ and ϵ are given by (50) and (26) respectively. The solution of (66) and (67) for initial conditions $v_x(o) = v_y(o) = 0$ is

$$v_x = \frac{E_x}{B_z} \exp(- \varkappa \xi) \sin \varkappa \Omega \xi , \tag{68}$$

$$v_y = - \frac{E_x}{B_z} \left[1 - \exp(- \varkappa \xi) \cos \varkappa \Omega \xi \right] , \tag{69}$$

where

$$\xi = \frac{\nu_c}{\nu_I} \ln \left[\epsilon_o \exp\left(\frac{\nu_I}{\nu_c} \tau\right) + (1 - \epsilon_o) \right] \tag{70}$$

rather than τ provides the parameter on the stream lines of the flow. The x and y components of the current density are then given by (55) and (56) with the dimensionless time τ replaced by ξ as given by (70), and together with $v_x(\xi)$ and $v_y(\xi)$ given by (68) and (69) provide the solution of the coupled momentum and current equations for the case where $\nu_c/\nu_I << 1$ and where the velocity of the plasma is not negligible during the ionization of the plasma. The frequency $\Omega^2 \omega_p/(1+\Omega^2)$ of the oscillations of the current density and displacement of the plasma with respect to time on a stream line is approximately proportional to the proton gyro-frequency if the Hall parameter is greater than unity. If $\Omega << 1$ this frequency is $\Omega^2 \omega_p$, but the latter case is not likely to be of interest here because the conditions of strong field and dominance of the Lorentz force over the pressure gradients presumed in Section 3.2.3 are probably not compatible with very small values of the Hall parameter.

3.2.5   Discussion

We have analyzed the MPD arc for the case of a strong applied magnetic field by means of an analytical model which assumes steady flow, charge neutrality, incompressibility, uniform electric and magnetic fields, considers only electromagnetic forces in both the momentum and the current equation and neglects the self field of the arc currents. The analysis, carried out in Lagrangian coordinates, yields the plasma motion and current density as a function of the initial coordinates and time following the motion of a plasma element. If the solution, which has been obtained for plane parallel electrodes with crossed electric and magnetic fields, is applied to a coaxial geometry, a plasma element is found to follow a spiraling motion with superimposed damped radial and azimuthal spatial oscillations. In the case for which the gas is strongly ionized before the plasma velocity is significant the azimuthal Hall and radial components reach the values $j_r = j_\theta/\Omega$ during the ionization. When the gas is strongly ionized the Hall component and the axial magnetic field produce a radial force which results in an acceleration of the plasma toward the axis. This radial motion tends to damp the Hall current which in turn has the effect of permitting the radial current to increase, even when the Hall parameter is large. The torque on the flow produced by the radial current flow causes an azimuthal acceleration which subsequently damps the radial current; the continued damped oscillations of the current and velocity components are given by equations (57) to (60). The damped oscillatory radial motion tends to zero velocity with a net displacement toward the axis of the configuration and the azimuthal motion tends to the the drift velocity E_r/B_z.

The presence of radial pressure gradients of course could alter the motion and current distribution obtained here. Rather strong radial gradients would be necessary in order to be significant compared with the Lorentz force, possibly 20 mm/cm or more. Malliaris[6] has measured cathode tip and arc chamber pressure under strong field conditions similar to those considered here. But the pressure distribution in the region of radial flow, where

this analysis applies, is not known. It seems unlikely that initially pressure gradients could develop which would be of sufficient magnitude to suppress the initial inward radial motion, and the other approximations should also hold reasonably well for small times. Hence we view with some confidence the qualitative aspect of the initial damping and enhancement of the radial current when the Hall parameter is large as displayed by our analytical model. However, it is a matter of conjecture whether the continued spatial oscillations of velocity and current density actually occur in the plasma flow. The consequence of the compressibility of the flow are difficult to see. To include compressibility effects in a meaningful way would require accounting for pressure gradients and probably induced fields and the axial acceleration of the flow which would go essentially beyond the crude level at which the problem has been dealt with here. Although the axial acceleration has not been treated directly it is of course connected with aspects of the problem which have been considered. The radial and Hall components of the current calculated here induce azimuthal and radial components of the magnetic field both of which produce an axial Lorentz force. The azimuthal motion resulting from the radial current flow is in part recoverable through the axial Lorentz forces which would act in a diverging magnetic field.

In a coaxial geometry, when the radial displacements are of the dimension of the electrode radius, the plasma may move to the axis where the radial field is very weak, violating our assumption of a uniform field. However, if we take $E_x(x) = E_x(x_0) \frac{x}{x_0}$, which is perhaps a better representation of the field in this case, it can be shown that damped oscillatory motion still results but with a different frequency. A negative radial pressure gradient would tend to damp the oscillatory motion; however, we have not considered the pressure distribution which would be required to, say, critically damp the motion.

REFERENCES

1. A. C. Ducati, E. Muehlberger and R. P. Treat, "Exploratory Electromagnetic Thruster Research," Giannini Scientific Corporation, Contract NAS w-1513, Interim Report (March 1967).

2. A. C. Ducati, "Analysis of Losses in Plasma Acceleration," Giannini Scientific Corporation, Contract AF 49(638)-1743, Annual Report (Nov. 1967).

3. A small plexiglass tank designed for pulsed arc operation has been constructed at Princeton University. R. G. Jahn and K. E. Clark, "A Large Dielectric Vacuum Facility," Department of Aerospace and Mechanical Sciences, Princeton University, Princeton, New Jersey (1966).

4. A. C. Ducati, E. Muehlberger and J. P. Todd, "Design and Development of a Thermo-Ionic Electric Thrustor," Giannini Scientific Corporation, Contract NAS w-968, Interim Report 3QS025-968 (Feb. 1965).

5. A. C. Ducati, R. G. Jahn, E. Muehlberger and R. P. Treat, "Design and Development of a Thermo-Ionic Electric Thrustor," Giannini Scientific Corporation, Final Report NASA CR-5703 (May 1966).

6. A. C. Malliaris, "Phenomena in the Cathode Region of an MPD Accelerator," AIAA Journal, 5, 1325 (1967).

7. J. Burlock and D. R. Brooks, "Correlation of Coherent Oscillations and Hall Currents in the Linear Hall Accelerator," Applied Physics Letters, 7, 49 (1965).

8. R. Lovberg, "Physical Processes in the Magneto-Plasmadynamic Arc," University of California, San Diego, Second Semiannual Report, NASA Grant NGR-05-009-030 (March 1967).

9. A. V. Larson, "Experiments on Current Rotations in an MPD Engine," AIAA Paper No. 67-689, AIAA Electric Propulsion and Plasmadynamics Conference, Colorado Springs, Colorado (Sept. 1967).

10. H. Hügel, G. Kruelle and T. Peters, "Investigations on Plasma Thrusters with Thermal and Self-Magnetic Acceleration," AIAA Journal, 5, 551 (1967).

11. K. E. Clark, A. C. Eckbreth and R. G. Jahn, "Current Pattern Stabilization in Pulsed Plasma Accelerators," AIAA Paper No. 67-656, Electric Propulsion and Plasmadynamics Conference, Colorado Springs, Colorado (Sept. 1967).

REFERENCES (cont.)

12. A. C. Ducati and R. G. Jahn, "Design and Development of a Thermo-Ionic Electric Thrustor," Giannini Scientific Corporation, Interim Report 5QS085-968 (Aug. 1965).

13. W. E. Powers, "Measurements of the Current Density Distribution in the Exhaust of an MPD Arc Jet," AIAA Paper No. 66-116, 3rd Aerospace Sciences Meeting, New York, N. Y. (Jan. 1966).

14. A. M. Schneiderman and R. M. Patrick, "Optimization of the Thermal Efficiency of the Magnetic Annular Arc," AIAA Journal, 4, 1836 (1966).

15. N. M. Nerheim and A. J. Kelly, "A Critical Review of the State-of-the-Art of the MPD Thrustor," AIAA Paper No. 67-688, Electric Propulsion and Plasmadynamics Conference, Colorado Springs, Colorado (Sept. 1967).

16. W. E. Powers, "Measurements of the Current Density Distribution in the Exhaust of an MPD Arc Jet," AIAA Journal, 5, 545 (1967).

17. R. M. Patrick and A. M. Schneiderman, "Study of Magnetic Annular Plasma Accelerator," Avco Everett Research Laboratory, Contract NAS w-5748, Summary Report (Jan. 1966).

18. G. L. Cann, R. L. Harder, R. A. Moore and P. D. Lenn, "Hall Current Accelerator," EOS, Contract NAS w-5909, Third Quarterly Progress Report (March 1965).

19. J. L. Delcroix, Introduction to the Theory of Ionized Gases, Interscience, New York, N. Y., p. 133 (1960).